NASA Reference Publication 1072

Determination of Wind From Nimbus 6 Satellite Sounding Data

William E. Carle and James R. Scoggins

JANUARY 1981

NASA

NASA Reference Publication 1072

Determination of Wind From Nimbus 6 Satellite Sounding Data

William E. Carle and James R. Scoggins
Texas A&M University
College Station, Texas

National Aeronautics
and Space Administration

**Scientific and Technical
Information Branch**

1981

ACKNOWLEDGMENTS

The authors extend thanks to Dr. Vance E. Moyer, Dr. Kenneth C. Brundidge, Mr. Keith Knight, and Dr. Jack A. Barnes for their suggestions and discussions during the preparation of this report, to Mr. John Rod for preparation of the figures, and to Mrs. Karen Hood for typing the final manuscript.

This research was supported by the U. S. Army Research Office, under Grant No. DAAG 29-76-G-0078 to the Department of Meteorology, Texas A&M University.

This report is published with the permission of the U. S. Army Research Office for use in connection with studies utilizing space technology for weather-related programs in progress in the Atmospheric Sciences Division, Space Sciences Laboratory, NASA, Marshall Space Flight Center.

TABLE OF CONTENTS

TABLE OF CONTENTS (Continued)

LIST OF TABLES

LIST OF FIGURES

LIST OF FIGURES (Continued)

LIST OF FIGURES (Continued)

LIST OF FIGURES (Continued)

DETERMINATION OF WIND FROM NIMBUS-6 SATELLITE SOUNDING DATA*

William E. Carle and James R. Scoggins
Department of Meteorology
Texas A&M University

1. INTRODUCTION

a. Statement of problem

Detailed knowledge of atmospheric motion on a global scale is important for diagnostic and forecasting purposes. Atmospheric motion is measured with the current rawinsonde network only over land areas, leaving vast ocean areas unsampled. Gaps exist in the knowledge of atmospheric motion over the oceans and even over land areas where there are large distances between rawinsonde stations. The knowledge of atmospheric motion could be significantly improved by using wind fields derived from satellite sounding data if these data are of sufficient accuracy. A polar-orbiting satellite can sample the atmosphere over the entire globe twice each day with smaller distances between soundings than the current rawinsonde network. Methods of determining atmospheric winds from satellite sounding data need to be developed.

This study describes methods of determining wind on constant-pressure charts and in the boundary layer from satellite thermodynamic data. Wind fields are computed in four geographical regions from soundings of temperature and moisture obtained from Nimbus-6 satellite radiance measurements.

b. Objectives

The primary objective of this research is to develop objective methods of computing upper-level and surface wind fields from satellite sounding data. Evaluations of these methods will be based on

---

* Research supported by U. S. Army Research Office, Research Triangle Park, North Carolina, under Grant DAAG 29-76-G-0078 to the Department of Meteorology, Texas A&M University.

comparisons between rawinsonde winds and winds derived from Nimbus-6 satellite sounding data over several geographical regions of varying synoptic conditions. Kinematic parameters from satellite-derived and rawinsonde winds will be compared to further evaluate the methods of computing wind from satellite soundings.

c. Previous studies

Suchman and Martin (1976) determined wind from satellite data by computing cloud motions from visual and infrared satellite images. Cloud positions were transformed into coordinates of latitude and longitude, and cloud velocity was computed from cloud motion relative to the earth. Cloud-top temperatures were determined from satellite-measured radiances. Cloud heights were estimated using the standard atmosphere relationship between temperature and height. Winds derived from cloud motions were assumed to be valid at the cloud-top heights, but it was uncertain how much error was made in estimating heights. Other uncertainties cited by Hubert and Whitney (1971) include nonadvective cloud motions and errors in tracking. The dominant circulation features observed in rawinsonde winds were recognizable in the fields of satellite winds. The wind could be calculated only at the highest cloud level when thick high-level clouds obscured the view of low-level clouds. Therefore, the vertical profile of wind remained poorly defined. Thomasell (1979) described an objective wind analysis model for processing and evaluating wind fields on a latitude-longtitude grid.

Horizontal winds may be determined from satellite thermodynamic data rather than from cloud motions. A capability was developed to derive vertical profiles of temperature and water vapor content from satellite-measured radiances (Smith et al., 1972). These vertical profiles may be used to compute gradients of temperature or geopotential height which may then be converted into a satellite-derived wind field.

The accuracy of satellite-derived winds computed on cross sections or on constant-pressure charts is normally judged by comparing the satellite winds with similar fields of rawinsonde winds.

Kapela and Horn (1975), using both rawinsonde and Nimbus-5 sounding data, constructed isentropic cross sections through an intense baroclinic zone. Temperature gradients from the cross sections and the 850-mb geostrophic wind were used to obtain geostrophic and gradient wind components normal to the cross sections. Winds computed from satellite data compared favorably with rawinsonde winds but with a loss of detail. In general, the rms differences between gradient winds derived from Nimbus-5 data and rawinsonde winds were slightly smaller than the rms differences between rawinsonde winds and gradient winds derived from rawinsonde sounding data. Maximum wind speeds in the cross sections of observed winds, gradient winds from rawinsonde data, and gradient winds from Nimbus-5 data were within 2 m s^{-1}. In a similar study (Horn et al., 1976), isentropic cross sections were constructed from Nimbus-5 soundings, radiosonde observations, and the initial-hour output of the Limited-area Fine Mesh (LFM) model. The Nimbus-5 geostrophic wind fields computed from 1700 GMT data fit nicely between the 1200 and 0000 GMT radiosonde and LFM wind fields. It was shown that the location and intensity of strong wintertime jet maximums could be derived from satellite sounding data.

Smith et al. (1975) used Nimbus-5 soundings to obtain geostrophic wind components perpendicular to cross sections in four separate case studies. Their satellite-derived geostrophic winds showed good correspondence with observed winds as well as geostrophic winds derived from radiosonde data. In another study (Arnold et al., 1976), geostrophic wind was computed from cross sections of radiosonde and Nimbus-5 data. Profiles of geostrophic wind were computed with the aid of a tie-on wind (an assumed wind somewhere in the profile to which thermal winds can be added). Again, general agreement was found between the two sets of wind fields but with a loss of detail in satellite-derived winds. Largest differences between the wind fields occurred near the tropopause and were dependent on the level at which a tie-on wind was used to compute geostrophic winds. It was suggested that a tie-on wind from cloud motion vectors might be an optimum approach.

In a recent study (Petersen and Horn, 1977), temperature profiles obtained from Nimbus-6 radiance measurements were used along with sea-level pressures to construct gridded fields of 500-mb geopotential height and geostrophic wind over northeastern North America. Satellite-derived winds obtained at 1600 GMT were compared with geostrophic winds computed from 1200 and 0000 GMT rawinsonde height analyses prepared by the National Meteorological Center (NMC). It was found that the isotach fields of geostrophic wind showed good continuity between satellite and bracketing NMC analyses. Locations of the 500-mb velocity maximums were reasonably consistent between the two data sets. The rms differences between satellite and NMC geostrophic wind fields ranged from 3.5 to 5.0 m s^{-1}, which are comparable to the differences observed between successive NMC analyses.

Moyer et al. (1978) compared geostrophic winds derived from Nimbus-6 and rawinsonde data for an August 1975 case over the central United States. Rawinsonde height measurements taken at 1200 and 0000 GMT were linearly interpolated in time and assumed to be representative of the 1700 GMT conditions when the Nimbus-6 satellite passed over the region. Geopotential heights derived from satellite data were computed by integrating the hydrostatic equation. Satellite temperatures were used in the integration. Geostrophic winds at nine levels were computed from gridded fields of rawinsonde and satellite-derived heights. Profiles of the average and standard deviation of differences between satellite and rawinsonde geostrophic wind speeds and directions were presented. Both the average and standard deviation of differences in wind speed increased with altitude. Average differences in geostrophic wind speed were less than 5 m s^{-1} at all altitudes, while the standard deviation increased from about 5 m s^{-1} at 850 mb to 10-12 m s^{-1} on constant-pressure surfaces above 400 mb. Average differences in wind direction generally were less than 20°. The standard deviation of differences in direction was relatively constant at about 40° from 850 to 300 mb, then increased to approximately 70° at 100 mb.

2. DATA UTILIZED

a. Rawinsonde and surface data

Rawinsonde and surface data for this study were obtained from the Texas A&M University archives of National Weather Service teletype data, and from the National Climatic Center. Rawinsonde data used include temperature, geopotential height, and wind speed and direction at mandatory levels at 1200 GMT on 25 August 1975, 0000 GMT on 26 August 1975, and 0000 and 1200 GMT on 3 September 1975. Surface hourly data used in the study include temperature, dew-point temperature, altimeter setting, and wind speed and direction at 1700 GMT on 25 August 1975, and 0700 GMT on 3 September 1975.

b. Satellite data

Satellite data used in this study were processed by the Goddard Institute for Space Studies and were provided by the National Environmental Satellite Service. The data include temperature and dew-point temperature at 21 pressure levels (1000, 950, 920, 850, 780, 700, 670, 620, 570, 500, 475, 430, 400, 350, 300, 250, 200, 150, 135, 115, and 100 mb) at 1700 GMT on 25 August 1975, and 0730 GMT on 3 September 1975. Also included are the latitude, longitude, and the approximate surface elevation for each sounding.

Vertical and horizontal smoothing exist in the sounding data. Temperatures are retrieved from radiances measured by the High Resolution Infrared Radiation Sounder (HIRS) and the Scanning Microwave Spectrometer (SCAMS) flown on the Nimbus-6 satellite. Temperature is determined from the energy emitted in each wavelength band, and applied to a particular level in the atmosphere depending on the characteristics of the weighting function for that wavelength band. The temperature so obtained, although applied at a single pressure level, represents energy emitted from all levels in the atmosphere so that vertical smoothing is present in the soundings. The large area field of view (scan swath) represented by the satellite sounding introduces horizontal smoothing.

An important characteristic of the satellite soundings is the lack of surface data other than elevation. In order to establish reasonable surface conditions for the satellite soundings, hourly surface observations were used (in combination with the estimated elevation and location of each sounding) to estimate actual surface temperature, dew-point temperature, and pressure. Altimeter setting, temperature, and dew-point temperature from surface observations at the time of the satellite pass were plotted and analyzed. The three surface parameters were then spatially interpolated from the analyzed fields to each of the satellite sounding locations. The interpolated surface temperature and dew-point temperature were used as the surface values at each satellite sounding location. The altimeter setting, interpolated to each satellite sounding location, was converted to station pressure based upon the surface elevation at the location.

Station pressure and altimeter setting are related by

$$P = ALT - \Delta P$$

where P is station pressure, ALT is altimeter setting, and ΔP is the difference in pressure in the standard atmosphere between the station and standard sea-level pressure (i.e., 1013.25 mb).

Hydrostatic equilibrium is assumed so that

$$\frac{dP}{dZ} = - \frac{gP}{RT}.$$

With lapse rate B, and sea-level temperature T_0, the temperature at height Z may be expressed as

$$T = T_0 - BZ.$$

The relation between pressure and elevation is found by substituting the expression for temperature into the hydrostatic relation and integrating. This gives

$$P_1 = P_0 \left(1 - \frac{BZ}{T_0}\right)^{gR^{-1}B^{-1}}$$

where Z (in meters) is the elevation of the satellite sounding location and P_0 is sea-level pressure.

Since P_1 is surface pressure in the standard atmosphere and B is the standard atmospheric lapse rate ($6.5°C\ km^{-1}$), we have

$$P_1 = 1013.25\ (1 - \frac{0.0065\ Z}{288})^{5.26}$$

and ΔP can be defined as

$$\Delta P = P_0 - P_1 = 1013.25\ (1-(1- \frac{0.0065\ Z}{288})^{5.26}).$$

Station pressure, temperature and dew-point temperature interpolated from the hourly surface observations, and elevation supplied with the satellite data complete the surface data needed for each satellite sounding location.

3. AREAS SELECTED FOR ANALYSIS AND DISTRIBUTION OF DATA

Four geographic regions were chosen for analysis in this research. The regions were selected on the basis of data availability and synoptic conditions. The Nimbus-6 satellite passed over the central United States at approximately 1700 GMT on 25 August 1975. From this pass three regions were selected: 1) central United States; 2) Caribbean Sea; and 3) central Canada. Locations of rawinsonde soundings, satellite soundings, and surface wind observations for these three regions are shown in Figs. 1-3. Data coverage is greatest for the central United States region. In this region there are 39 rawinsonde soundings, 39 satellite soundings, and 203 surface wind observations. Rawinsonde and satellite soundings are about evenly distributed over the region. Surface data are much more dense than the upper-level data and are more evenly distributed. Data for the Caribbean region include 28 rawinsonde soundings, 43 satellite soundings, and 110 surface wind observations. While satellite data for this region are about evenly distributed, rawinsonde and surface data are sparse in the Gulf of Mexico. Data for the Canada region include 22 rawinsonde soundings, 33 satellite soundings, and 134 surface wind observations. Data are about evenly distributed in this region.

The fourth region selected for analysis is the western United States. Locations of rawinsonde and satellite soundings for the western United States region are shown in Fig. 4. The Nimbus-6 satellite passed over the region at approximately 0730 GMT on 3 September 1975. Data for this region include 35 rawinsonde and 34 satellite soundings. Satellite and rawinsonde soundings are about evenly distributed over the region. Surface wind was not analyzed in this region.

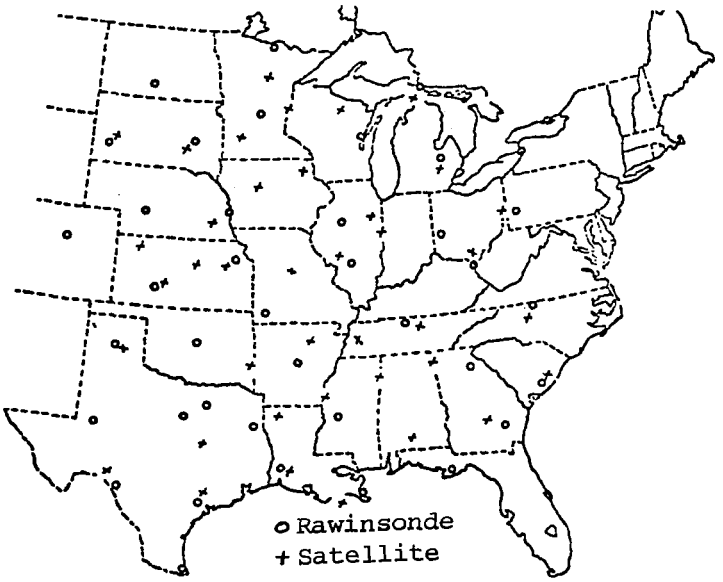

a. Locations of soundings

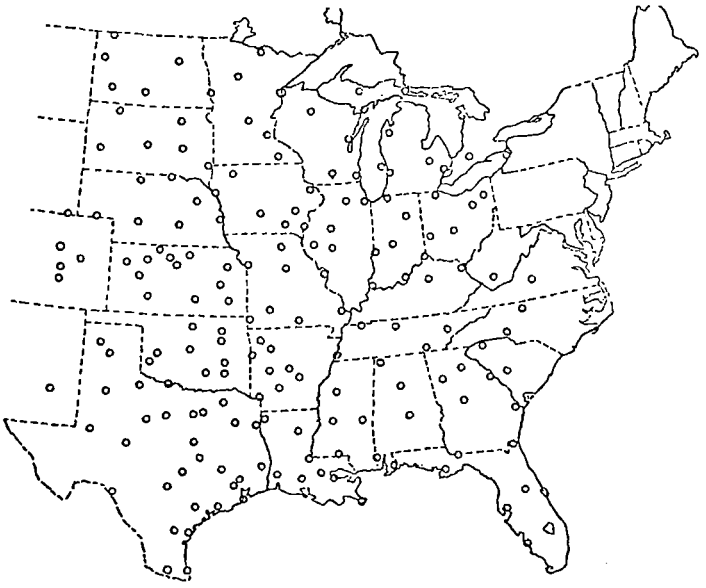

b. Locations of surface wind observations

Fig. 1. Locations of rawinsonde and satellite soundings and surface wind observations in the central United States region.

a. Locations of soundings

b. Locations of surface wind observations

Fig. 2. Locations of rawinsonde and satellite soundings and surface wind observations in the Caribbean region.

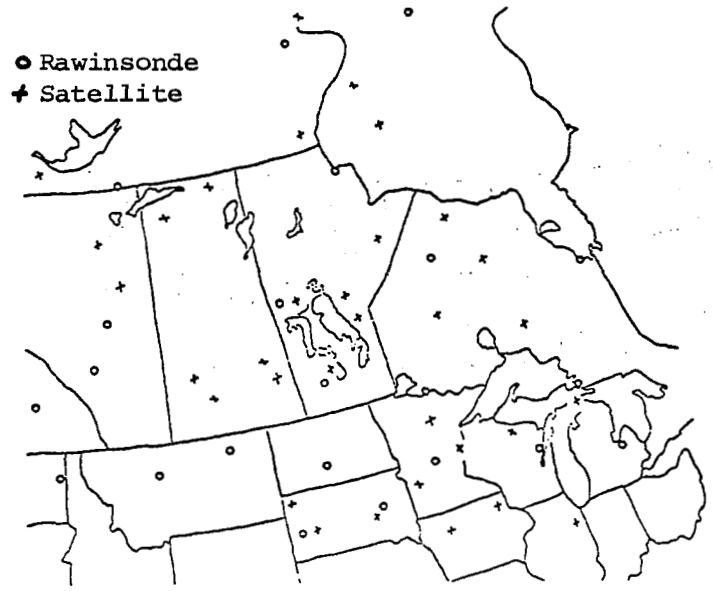

a. Locations of soundings

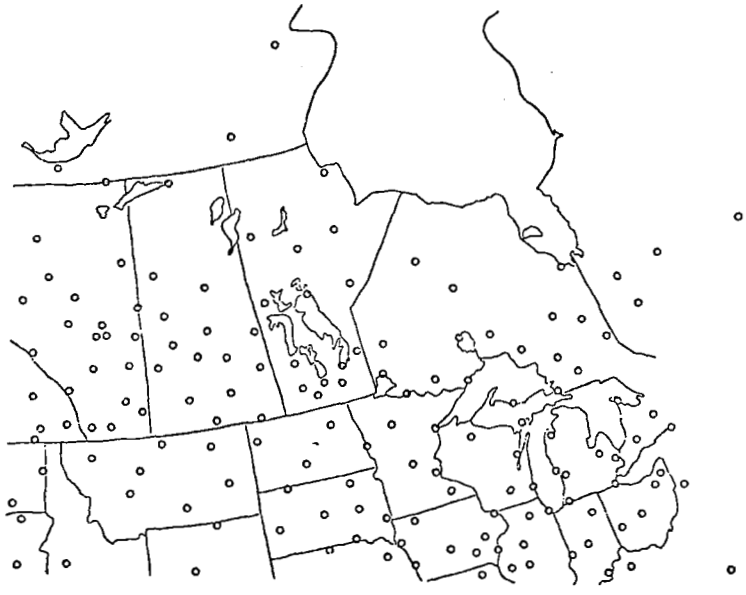

b. Locations of surface wind observations

Fig. 3. Locations of rawinsonde and satellite soundings and surface wind observations in the Canada region.

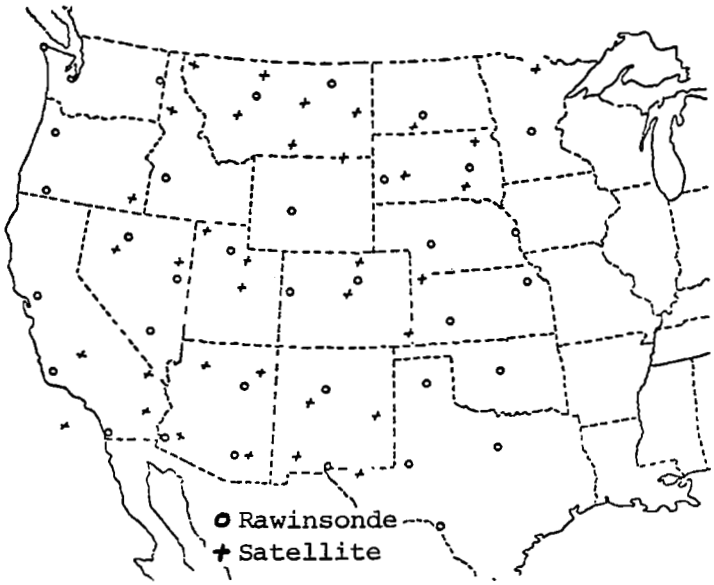

Fig. 4. Locations of rawinsonde and satellite soundings in the western United States region.

4. SYNOPTIC CONDITIONS

Synoptic charts for the central United States region are shown in Fig. 5 for the surface at 1800 GMT on 25 August 1975, and for 700, 500, and 200 mb at 1200 GMT. Synoptic charts for the Caribbean and Canada regions are shown in Figs. 6 and 7 for the surface at 0000 GMT on 26 August 1975, and for 700, 500, and 200 mb at 1200 GMT on 25 August 1975.

At 1700 GMT on 25 August 1975, a strong low-pressure system was centered on the southern edge of Hudson Bay. A surface cold front extended from the low across the Great Lakes, Wisconsin, eastern Iowa, Missouri, southeastern Kansas, the Texas Panhandle, and eastern New Mexico. A squall line in Illinois and Missouri and a low-pressure area in Oklahoma were associated with the cold front. A warm front extended from a short occlusion into southeastern Canada and the northeastern United States. A high-pressure area in the southeastern United States dominated the flow in the Southern States and in the Caribbean region. There was little significant weather in the Caribbean region. Horizontal gradients of pressure and temperature were large in Canada, moderate in the central United States, and small in the Caribbean.

Synoptic charts for the western United States are shown in Fig. 8 for the surface at 0900 GMT on 3 September 1975, and for 700, 500, and 200 mb at 1200 GMT. At 0730 GMT on 3 September 1975, a low-pressure center was located north of Minnesota with an associated occlusion extending into northern Iowa. A cold front extended southwest of the occlusion into Kansas and New Mexico. Most of the western United States was free from convective activity with only a few thunderstorms in Arizona and New Mexico. There was a high-pressure center in western Montana and a low-pressure center in southern California. Horizontal gradients of pressure and temperature were small in the western United States region.

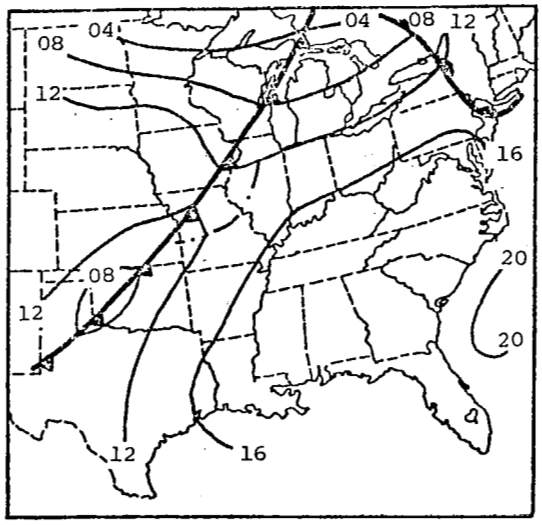

a. Surface chart at 1800 GMT

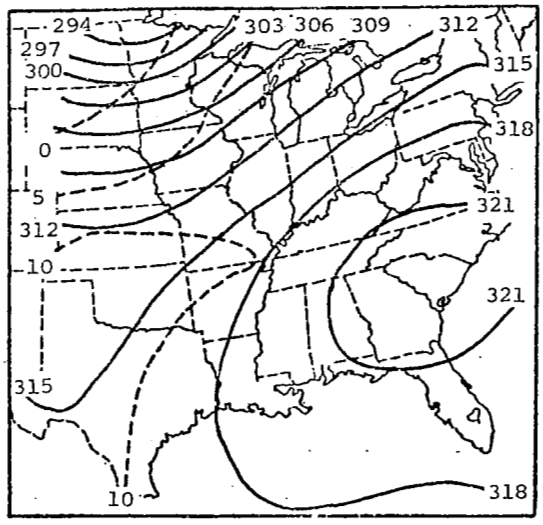

b. 700-mb chart at 1200 GMT

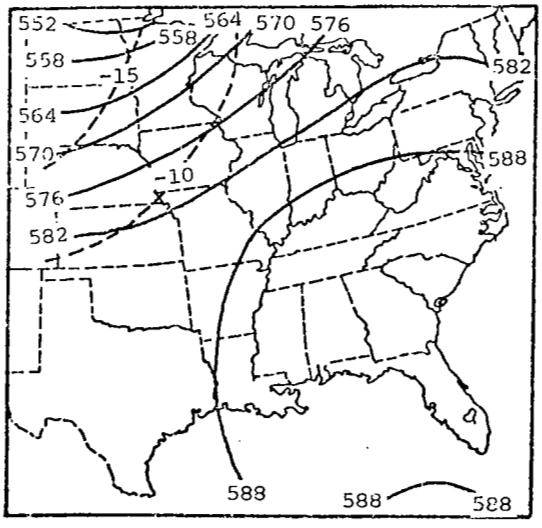

c. 500-mb chart at 1200 GMT

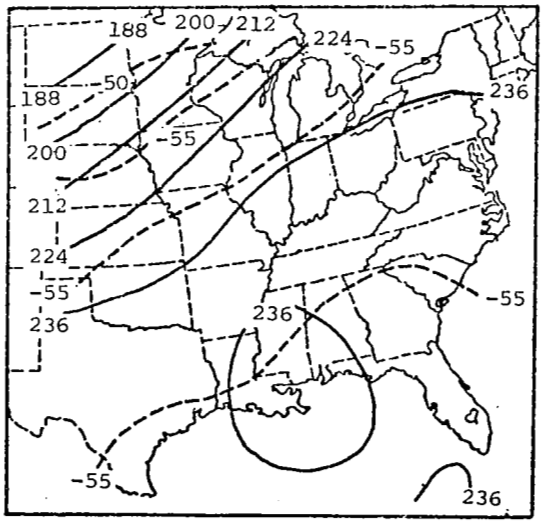

d. 200-mb chart at 1200 GMT

Fig. 5. Synoptic charts for the central United States region on 25 August 1975.

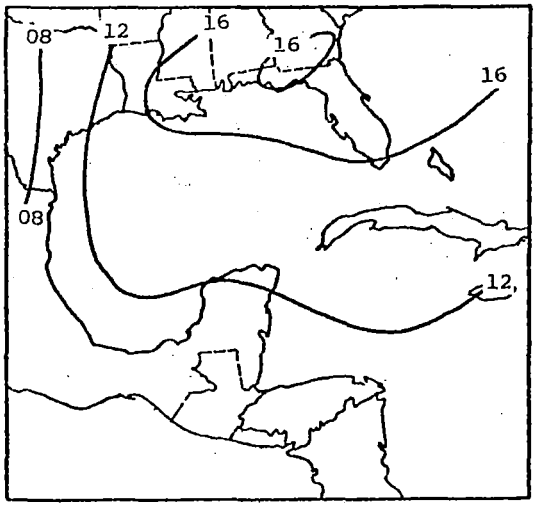

a. Surface chart at 0000 GMT on 26 August 1975

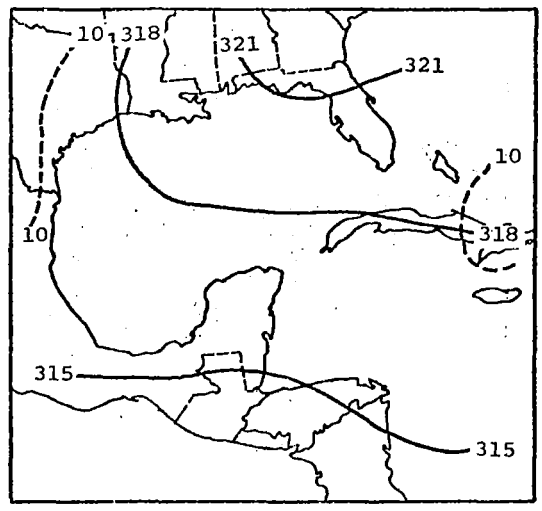

b. 700-mb chart at 1200 GMT on 25 August 1975

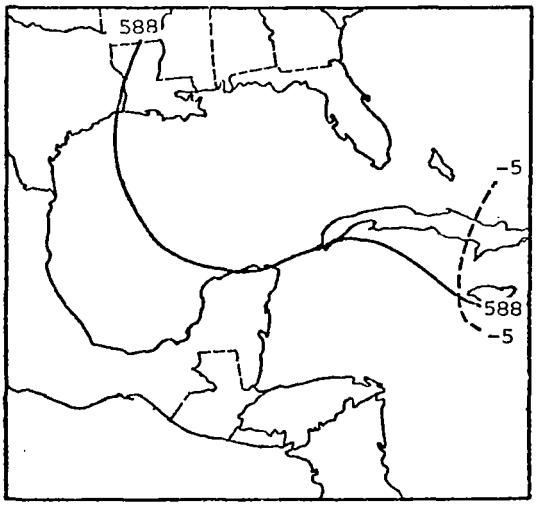

c. 500-mb chart at 1200 GMT on 25 August 1975

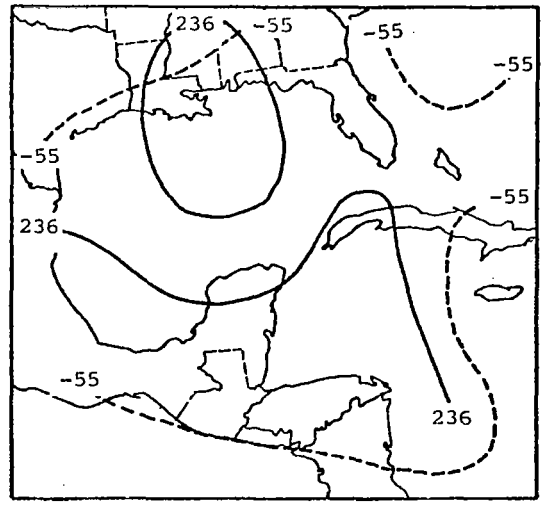

d. 200-mb chart at 1200 GMT on 25 August 1975

Fig. 6. Synoptic charts for the Caribbean region.

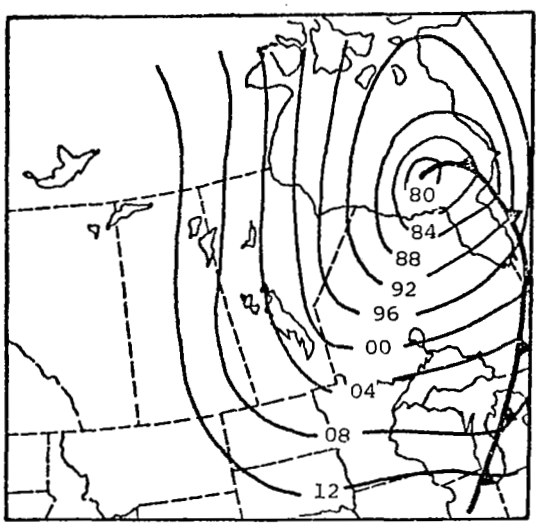

a. Surface chart at 0000 GMT on 26 August 1975

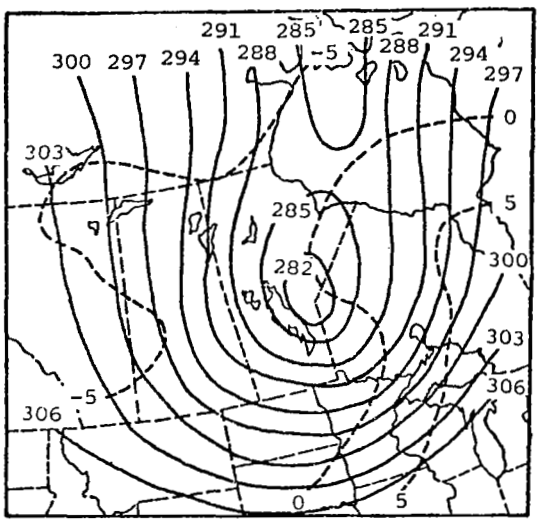

b. 700-mb chart at 1200 GMT on 25 August 1975

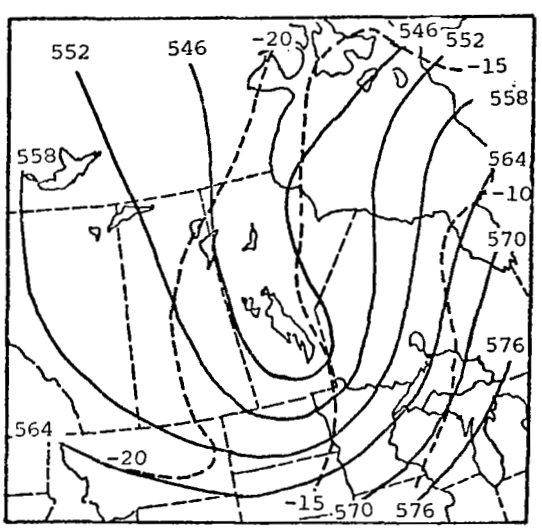

c. 500-mb chart at 1200 GMT on 25 August 1975

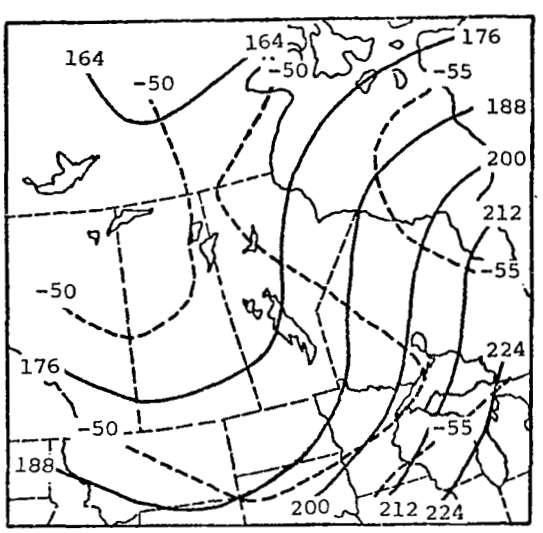

d. 200-mb chart at 1200 GMT on 25 August 1975

Fig. 7. Synoptic charts for the Canada region.

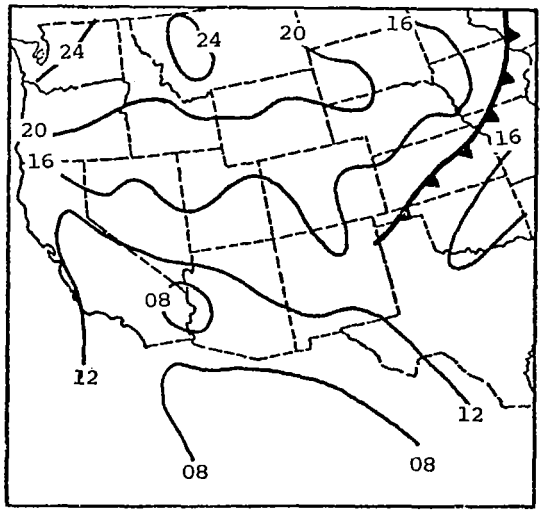

a. Surface chart at 0900 GMT

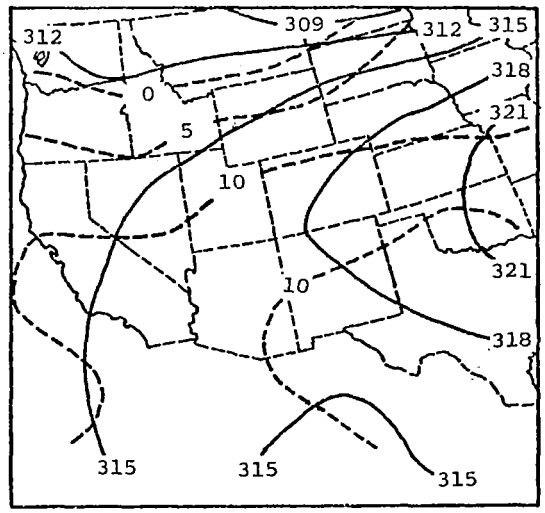

b. 700-mb chart at 1200 GMT

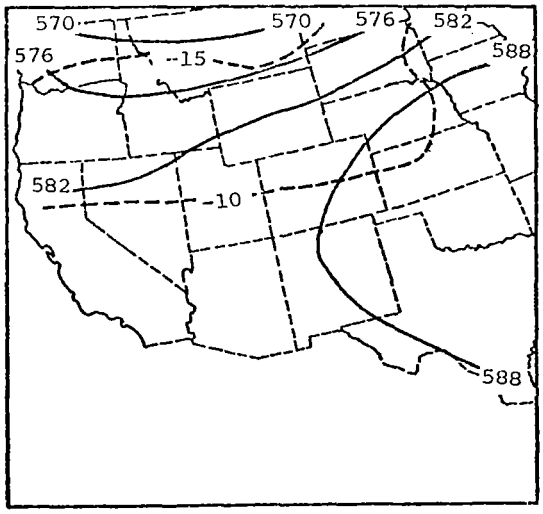

c. 500-mb chart at 1200 GMT

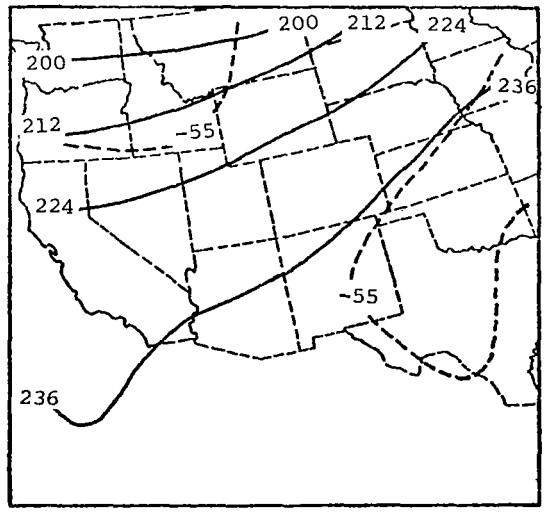

d. 200-mb chart at 1200 GMT

Fig. 8. Synoptic charts for the western United States region on 3 September 1975.

3. ANALYSIS PROCEDURE

a. Construction of gridded constant-pressure charts

Satellite-derived and rawinsonde winds are compared in this study to evaluate methods of computing winds from satellite sounding data. Two problems make it difficult to directly compare satellite and rawinsonde winds. Satellite and rawinsonde soundings are 1) not taken at the same time, and 2) not taken at the same locations. One approach to the first problem is to quantitatively compare satellite data with rawinsonde data from bracketing sounding times and to present two sets of differences. A second approach to the problem of nonsimultaneous data is to compare satellite data with rawinsonde data that have been linearly interpolated in time to represent the conditions at the time of the satellite pass. A method of dealing with the second problem is to compare paired soundings of satellite and rawinsonde data and to present differences as though the soundings are colocated. A second approach is to grid the satellite and rawinsonde data on constant-pressure surfaces and to compute differences between the data at the grid points. The second approach to dealing with both problems has been used in this study.

Rawinsonde data for the Caribbean, central United States, and Canada regions are linear time interpolations to 1700 GMT on 25 August 1975 from the 1200 and 0000 GMT soundings. The rawinsonde data for the western United States are linear time interpolations to 0730 GMT on 3 September 1975 from the 0000 and 1200 GMT soundings. Satellite data compare more favorably to interpolated rawinsonde data than to rawinsonde data from either of the bracketing times (Moyer, et al., 1978).

An objective analysis scheme developed by Barnes (1964) was used to interpolate rawinsonde and satellite data to a square grid of 324 points (18 x 18) with a grid-point spacing of 158 km. The gridding procedure is iterated four times and a scanning radius determines the maximum distance that a data point may influence the grid-point values. A nine-point smoothing routine (Shuman, 1957) was applied to each gridded field to reduce amplitudes of spurious high-frequency waves.

The gridding procedure, when used with the proper scanning radius and the smoothing routine, produces fields of data which are very similar to hand-analyzed charts. Rawinsonde data were gridded for mandatory levels; observed winds were gridded for the surface. Satellite data were gridded for each of the 21 pressure levels included in the satellite soundings. The locations of the grid points and axes of cross sections are shown in Fig. 9. The location of the northwest corner of the central United States, Caribbean, Canada, and western United States grids are, respectively: 105°W, 50°N; 100°W, 35°N; 120°W, 68°N; and 125°W, 50°N.

Scanning radii used in the gridding of data are presented in Table 1 and were determined by the distribution of data in each region. The fairly even spacing of satellite sounding locations allowed the use of a scanning radius of three grid distances for satellite data in all regions. Rawinsonde and surface data were most dense over the United States, somewhat more sparsely spaced in Canada, and very sparse in the southern portion of the Caribbean region. An increased scanning radius was used in areas with less dense data. Thus, rawinsonde data were gridded using a scanning radius of three grid distances in the United States regions, four grid distances in the Canada region, and three grid distances near the United States coast and five grid distances in the southern two-thirds of the Caribbean region.

Table 1. Scanning radii (grid distances) used in the gridding of data for the four regions.

Region	Satellite data	Rawinsonde data	Surface winds
Central United States	3	3	2
Caribbean	3	3 or 5	3 or 5
Canada	3	4	2 or 3
Western United States	3	3	not used

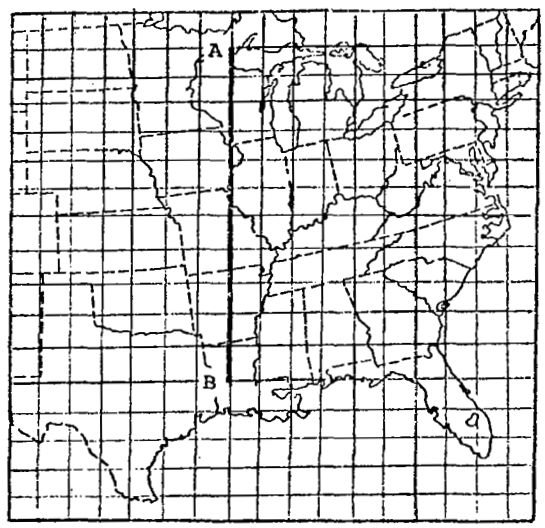

a. Central United States

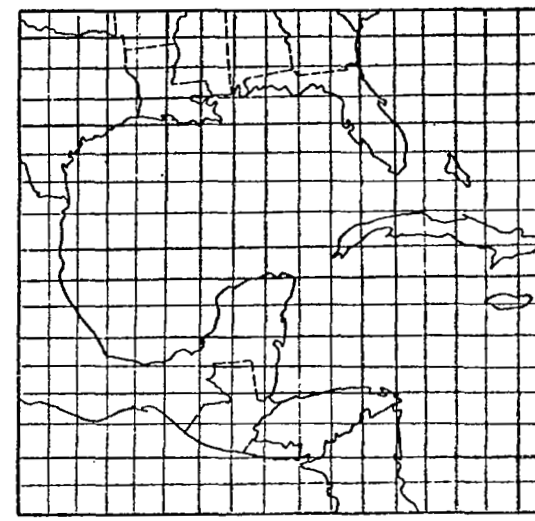

b. Caribbean

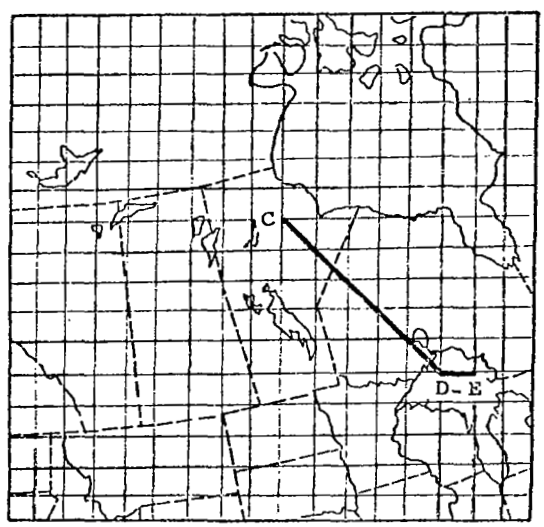

c. Canada

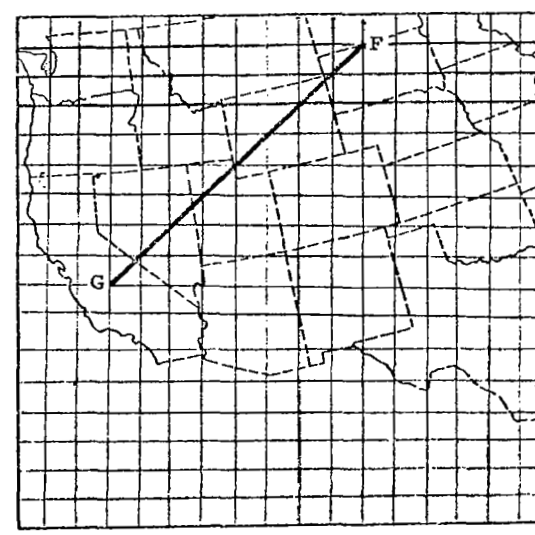

d. Western United States

Fig. 9. Computational grids and axes of cross sections.

Surface winds were gridded with a scanning radius of two grid distances in the central United States. Surface winds in the Caribbean were gridded in the same manner as rawinsonde data in that region. In Canada, surface winds were gridded with a scanning radius of two grid distances in the southern two-thirds of the region and three grid distances in the northern third.

The 0000 and 1200 GMT rawinsonde data were gridded and grid-point values linearly interpolated to correspond in time to the satellite pass. Wind direction was interpolated through the smaller angle.

b. Computation of geopotential height and geostrophic wind

Fields of geopotential height were computed from gridded satellite data by integrating the hydrostatic equation from the surface upward. In the integration process, mean virtual temperature for each layer was defined as the arithmetic average of the values at the top and bottom of the layer. Results were not improved by more involved methods. Surface temperature, dew-point temperature, and pressure were obtained from hourly synoptic data as explained previously.

Fields of geostrophic wind were computed from gradients of geopotential height at mandatory levels, viz., 850 (excluded in the western United States), 700, 500, 400, 300, 250, 200, 150, and 100 mb. Centered finite differences were used to compute the gradient of height. Correspondence between satellite-derived and rawinsonde winds was improved by applying a nine-point smoothing routine (Shuman, 1957) to the gridded height fields prior to computation of geostrophic winds.

c. Computation of gradient wind

Gradient wind was computed from the satellite-derived fields of geopotential height. It was hoped that the gradient wind approximation would yield better results than geostrophic wind wherever centripetal acceleration was significant. Gradient wind components were computed

according to

$$u_{gr} = u_g - \frac{k_1 k_2}{f}\left(u_g \frac{\partial v_g}{\partial x} + v_g \frac{\partial v_g}{\partial y}\right)$$

and

$$v_{gr} = v_g + \frac{k_1 k_2}{f}\left(u_g \frac{\partial u_g}{\partial x} + v_g \frac{\partial u_g}{\partial y}\right).$$

Here u_{gr} and v_{gr} are the gradient wind components, u_g and v_g are the geostrophic wind components, f is the Coriolis parameter, and k_1 and k_2 assume the following values:

k_1 = 0.1, 0.2, 0.2, 0.2, 0.2, 0.3, 0.4, 0.3, 0.3 for the 850, 700, 500, 400, 300, 250, 200, 150, and 100 mb surfaces, respectively, and

$$k_2 = \frac{\text{Sin L} - \text{Sin } 20^\circ}{\text{Sin } 30^\circ - \text{Sin } 20^\circ},$$

where L is latitude.

Values for k_1 and k_2 were determined empirically from rawinsonde data by the National Weather Service (1971) which uses these equations in the initialization of wind fields for the 6-layer (PE) numerical model. Arnason et al. (1962) derived the same expressions for gradient wind without factors k_1 and k_2 by considering a steady-state system and neglecting friction and vertical advection. In the present research, gradient winds also were computed using iterative methods and various values for the factors k_1 and k_2 without improving results.

d. Computation of wind through the boundary layer to the surface

Wind speed and direction through the boundary layer to the surface were computed from gridded fields of geopotential height. The u and v components of wind were assumed to vary linearly with height above 150 m and wind speed was assumed to have a logarithmic profile below 150 m. Wind direction at a grid point was assumed to be constant through the boundary layer. The logarithmic wind law is (Hess, 1959)

$$u = \frac{u_*}{k} \ln \frac{z}{z_o}$$

where k is the von Karman constant, z_o is roughness length, u_* is friction velocity, and u is wind speed at height z above the surface. When a value for wind speed (v_r) is known at reference height z_r, and

$z_r \leq 150$ m, surface wind speed, v_s, may be computed according to

$$v_s = \left(\frac{\ln z_s - \ln z_o}{\ln z_r - \ln z_o}\right) * v_r$$

where z_s is height of the surface wind.

Surface wind speed was computed for a height of 10 m. A value of 0.5 m was used for roughness length in the central United States and Canada regions, and a value of 0.2 m was used in the Caribbean region. These values are in agreement with values presented by Fiedler and Panofsky (1972) and Garratt (1977). Surface wind was not computed in the western United States because of the large variability of terrain height in the region.

Fields of satellite-derived geostrophic wind were used to define a reference wind speed and direction at each grid point. Where geostrophic wind could be computed from centered finite differences of height within 150 m of the surface, geostrophic wind speed was used as the reference wind speed in the logarithmic wind law. The level of the geostrophic wind was used as the reference height in the logarithmic wind law, and geostrophic wind direction was assumed to be equal to wind direction at 10 m. Where geostrophic wind could not be computed within the boundary layer, it was computed at the three lowest pressure levels at which a height gradient existed. The u and v components of the geostrophic wind for the three levels were then linearly extrapolated to a height of 150 m by the method of least squares. Wind speed defined by u and v components of wind at 150 m was used as the reference wind speed in the logarithmic law with a reference height of 150 m. Wind direction defined by u and v components at 150 m was assumed constant below 150 m.

e. Computation of kinematic parameters

Kinematic parameters were computed from gridded fields of rawinsonde and satellite data for each of the four regions. Horizontal advection of temperature, the vertical component of relative vorticity, and the horizontal advection of absolute vorticity were computed. The

rawinsonde calculations used fields of temperature and wind from rawinsonde measurements, while the satellite calculations used fields of temperature and geostrophic wind from satellite data.

6. RESULTS

a. Geostrophic wind

Satellite-derived geostrophic wind fields are compared to rawinsonde wind fields by three methods: 1) vertical profiles of differences between satellite-derived and rawinsonde wind fields; 2) constant-pressure charts of satellite-derived and rawinsonde wind fields and their differences; and 3) cross sections of the wind fields and their differences. Differences between satellite-derived and rawinsonde values are computed by subtracting rawinsonde from satellite values at the grid points. Thus, positive differences mean satellite-derived values are larger than rawinsonde values. The average difference and the standard deviation of the differences between satellite-derived and rawinsonde values are computed on nine constant-pressure surfaces (850, 700, 500, 400, 300, 250, 200, 150, and 100 mb). Vertical difference profiles consisting of the average and standard deviation of the differences are presented for each of the four regions. Only those grid points within one scan radius of both satellite and rawinsonde soundings were used in the computation of the average and standard deviation of the differences.

The average difference between satellite and rawinsonde values represents a bias in the satellite data relative to the rawinsonde data. If the profiles of these biases are pressure-dependent or associated with a synoptic situation, a correction factor could be used in future studies to eliminate the bias. The standard deviation of the differences is a measure of the variation in the magnitudes of the differences between satellite and rawinsonde values on a constant-pressure surface. Large standard deviations indicate that satellite-derived wind fields compare poorly with rawinsonde wind fields.

Following the vertical difference profiles are constant-pressure charts and cross sections analyzed for satellite-derived and rawinsonde wind fields and their differences. These were constructed from grid-point values on constant-pressure surfaces and represent the horizontal and vertical variations of the wind fields and their differences.

1) Vertical difference profiles

A nine-point smoothing routine (Shuman, 1957) was applied to the satellite-derived height fields over four grid distances with a smoothing parameter of 0.5. Effects of smoothing satellite-derived height fields before computing geostrophic wind fields are shown in Figs. 10 and 11. The differences between satellite geostrophic wind fields computed from smoothed fields of height and rawinsonde wind fields are shown by solid lines; similar differences resulting from unsmoothed satellite height fields are shown by dashed lines. Magnitudes of the average difference between satellite-derived geostrophic and rawinsonde wind speeds are decreased when satellite height fields are smoothed in three of the four regions. The exception is Canada where rawinsonde wind speeds are larger than satellite-derived geostrophic speeds computed from unsmoothed height fields. The smoothing process tends to decrease magnitudes of geostrophic wind speeds and, in Canada, this increases the magnitude of the average difference in wind speed. Differences in wind direction were, in general, decreased by the smoothing process as shown in Fig. 11. The magnitude of the standard deviation of the differences in wind direction was decreased more than the average difference.

Average differences between geostrophic wind speed computed from smoothed fields of satellite-derived height and rawinsonde wind speed are generally positive in the middle and upper troposphere as shown in Fig. 10. The exception to this is the Canada region where average differences between satellite-derived and rawinsonde wind speeds are negative at all levels below 150 mb. Mean differences range from about -5 to 5 m s^{-1} and are smallest in the Caribbean region where wind speeds are small at all levels. Magnitudes of the standard deviation of the differences in wind speed generally increase with altitude (decrease in pressure) until the level of maximum rawinsonde wind speed is reached. This level is between 150 and 200 mb in both United States regions, near 250 mb in Canada, and near 100 mb in the Caribbean. At this level, magnitudes of the standard deviation are approximately 11, 5, 11, and 12 m s^{-1} in the central United States, Caribbean, Canada, and western United States regions, respectively.

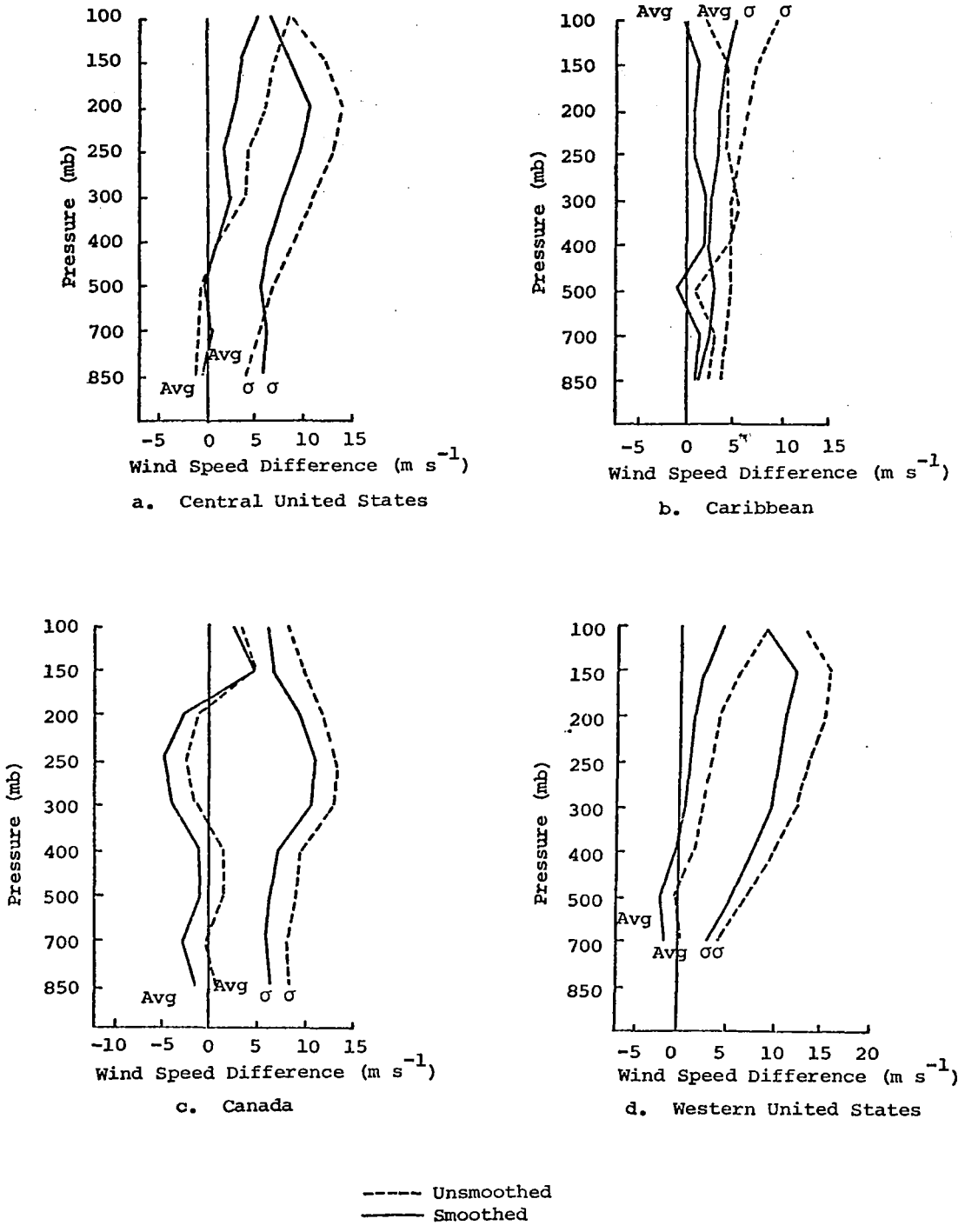

Fig. 10. Profiles of the average difference and standard deviation of the differences between satellite geostrophic wind speed computed from smoothed and unsmoothed heights and rawinsonde wind speed for four regions. Differences were computed by subtracting rawinsonde from satellite values.

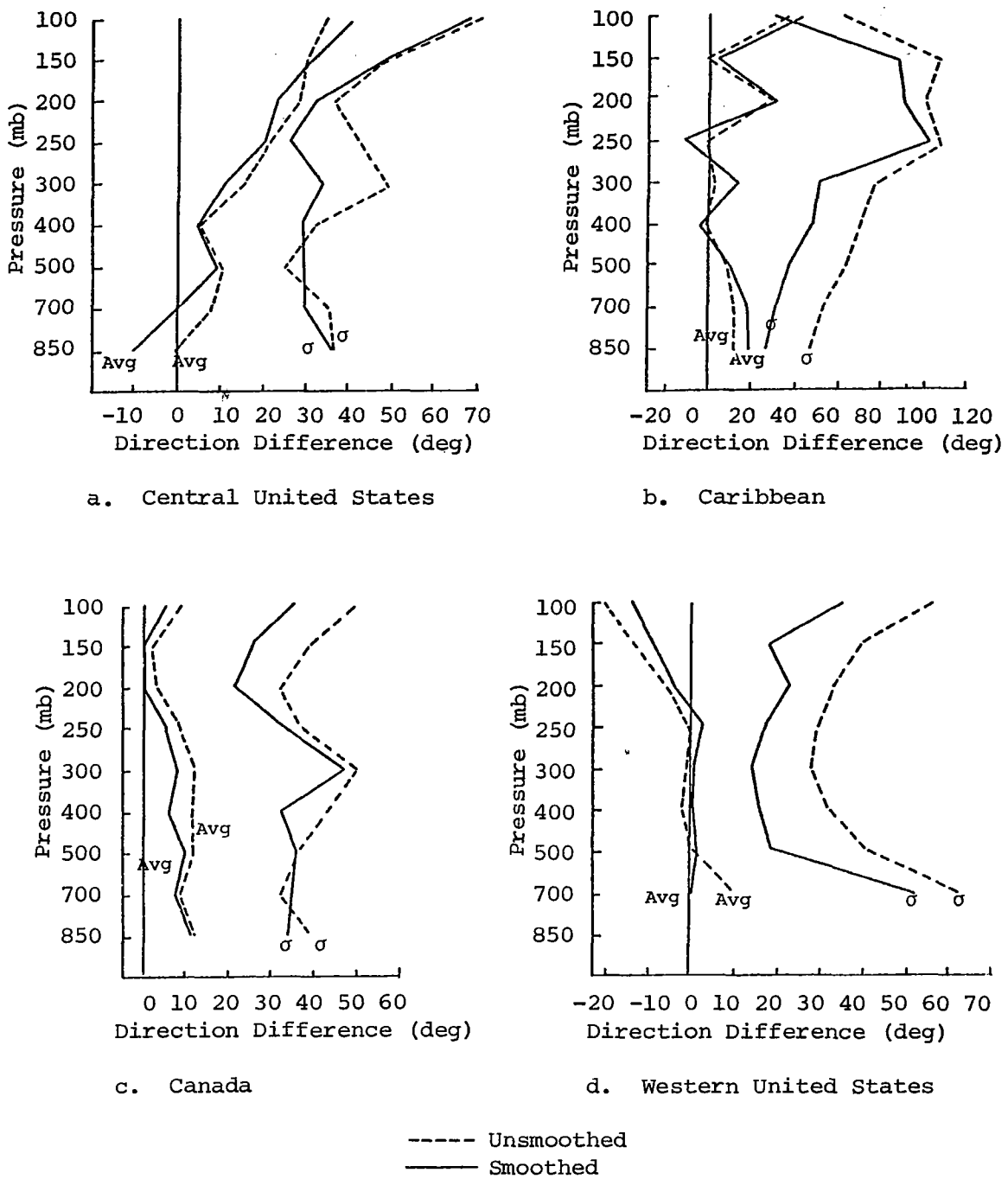

Fig. 11. Profiles of the average difference and standard deviation of the differences between satellite geostrophic wind direction computed from smoothed and unsmoothed heights and rawinsonde wind direction for four regions. Differences were computed by subtracting rawinsonde from satellite values.

The standard deviation of the differences in wind speed is between 3 and 12 m s^{-1} in the two United States regions and the Canada region, and varies from about 2 to 5 m s^{-1} in the Caribbean region.

Average differences and standard deviations of the differences between satellite geostrophic and rawinsonde wind directions, shown in Fig. 11, show the largest variation and generally large magnitudes in the Caribbean region where varying wind directions are associated with small wind speeds. Average differences in direction are between -12 and 41° in the Caribbean region and range from -14 to 40° in the other three regions. Magnitudes of the standard deviation of the differences in direction are between about 20 and 100° in the Caribbean region, and range from near 15 to 70° in the other three regions. Magnitudes of the standard deviation of the differences in direction are generally smallest near the level of maximum rawinsonde wind speed.

Vertical profiles of the differences between satellite-derived and rawinsonde u-component winds are shown in Fig. 12 for the four regions. Average differences in the u-component are positive on all constant-pressure surfaces for the central United States, and are generally negative for the other three regions. Average differences are between -5 and 5 m s^{-1} except in the central United States where the mean difference is approximately 7 m s^{-1} at 200 mb. Magnitudes of the standard deviation of the differences vary from about 2 to 10 m s^{-1} and are larger than the average differences at all levels in each of the four regions. Magnitudes of the standard deviation of the differences in the u-component tend to peak at the level of maximum wind speed.

Vertical profiles of the differences in the v-component of wind are shown in Fig. 13. The average difference is generally negative in the central United States and Canada regions, positive in the western United States, and fluctuates about zero in the Caribbean. The average difference is between -1 and 5 m s^{-1} in the Caribbean and western United States regions where wind speeds are small, and ranges from about -9 to 1 m s^{-1} in the other two regions. The magnitude of the standard deviation of the differences ranges from about 3 to 11 m s^{-1}

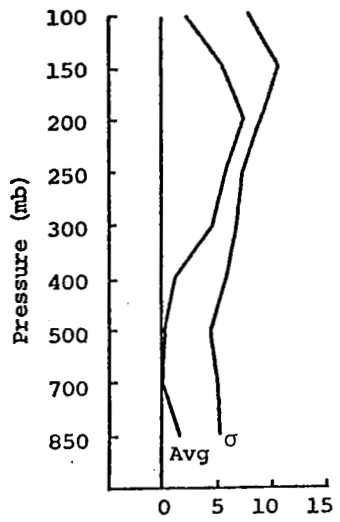

u-Component Difference (m s^{-1})

a. Central United States

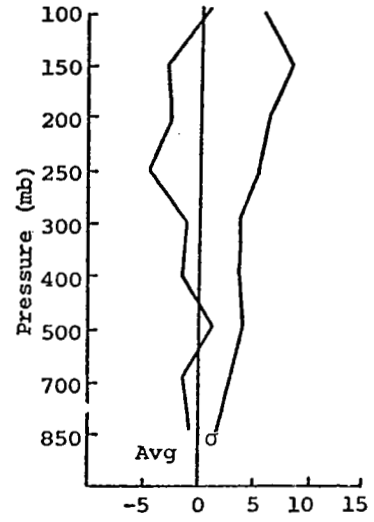

u-Component Difference (m s^{-1})

b. Caribbean

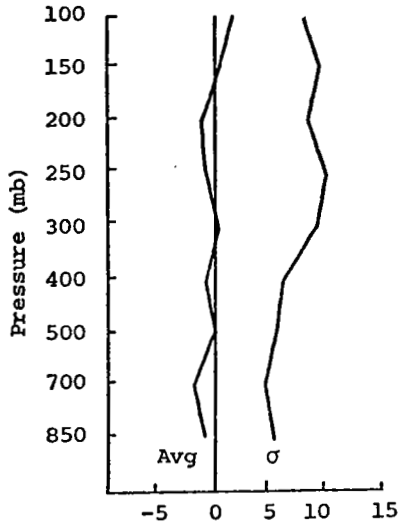

u-Component Difference (m s^{-1})

c. Canada

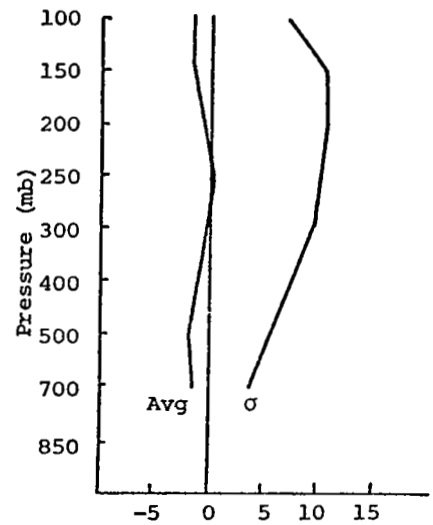

u-Component Difference (m s^{-1})

d. Western United States

Fig. 12. Profiles of the average difference and standard deviation of the differences between satellite geostrophic and rawinsonde wind u-component for four regions. Differences were computed by subtracting rawinsonde from satellite values.

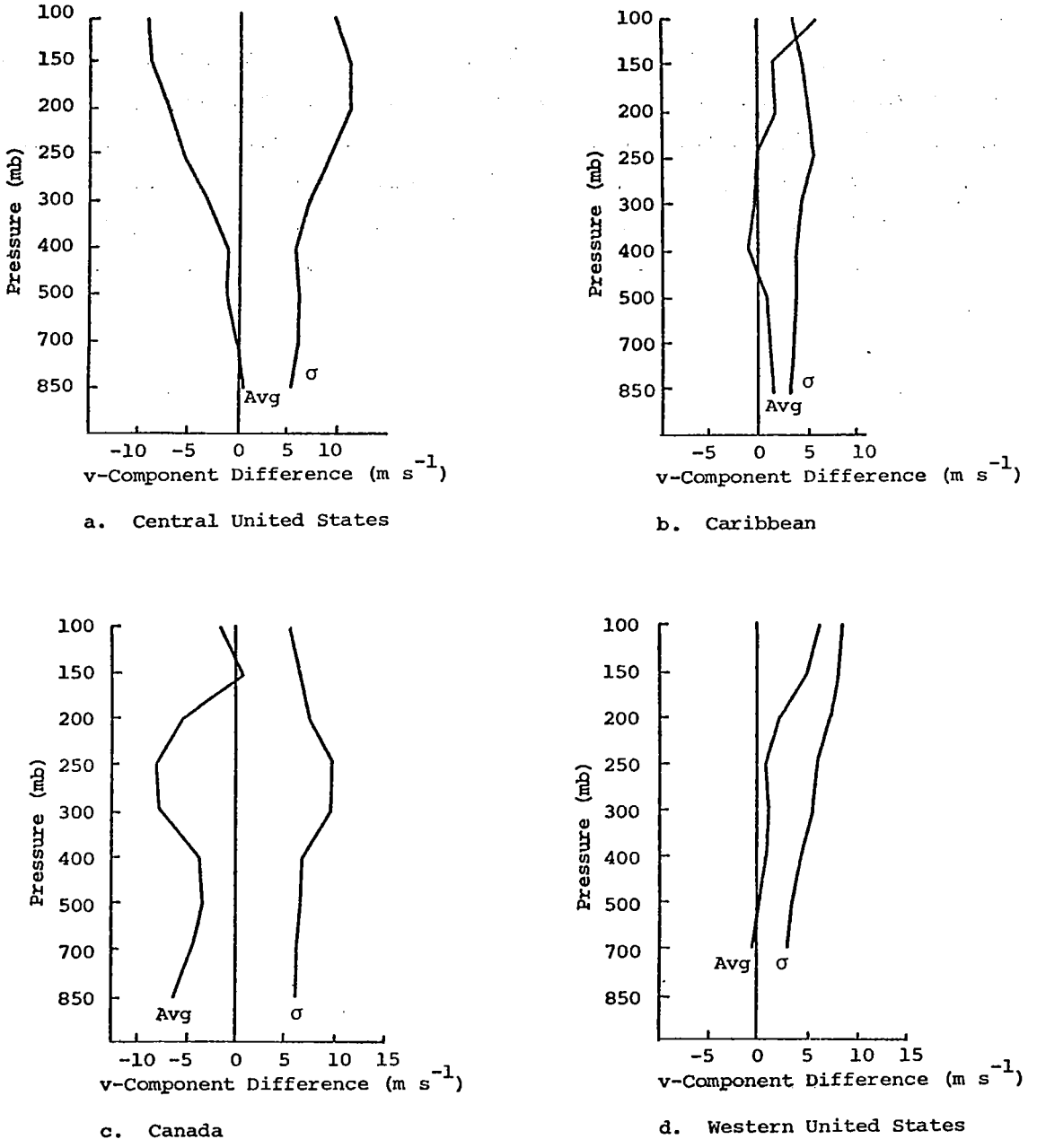

Fig. 13. Profiles of the average difference and standard deviation of the differences between satellite geostrophic and rawinsonde wind v-component for four regions. Differences were computed by subtracting rawinsonde from satellite values.

and is largest near the level of maximum wind speed in three of the four regions; the exception is the Caribbean where low wind speeds make the standard deviation of the differences less than 6 m s^{-1} at all levels.

Vertical profiles of the differences between geostrophic wind speeds derived from rawinsonde and satellite data have been presented by other investigators. Smith and Woolf (1974) derived vertical cross sections of geostrophic wind speed from rawinsonde and Nimbus-5 data. Moyer et al. (1978) compared geostrophic winds derived from gridded Nimbus-6 and rawinsonde data over the central United States. The results of these studies are presented in Fig. 14, along with representative (central United States) results from the present study. A comparison of the previous results with results from this study indicates that the standard deviations of differences between satellite-derived and rawinsonde wind speeds in the present study are generally smaller than values from geostrophic wind speeds in the previous studies. This difference may depend on the synoptic conditions in the area of consideration.

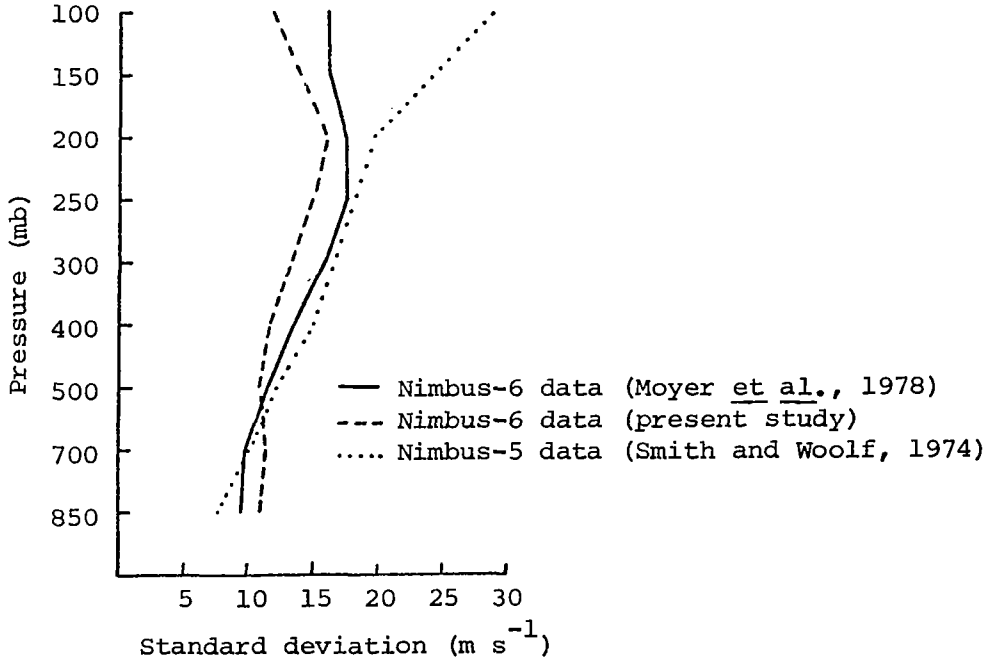

Fig. 14. Profiles of the standard deviation of differences between rawinsonde and Nimbus-5 and Nimbus-6 satellite-derived wind speeds.

Hubert and Thomasell (1979) compared rawinsonde and satellite-derived wind speeds in several meteorologically inactive regions. Satellite-derived wind speeds were computed from geostationary satellite measurements of cloud displacements. They found root mean square differences of 4.7 m s^{-1} for 900-mb wind and 8.5 m s^{-1} for upper-level winds at variable heights above 700 mb. These values are larger than those obtained in the present study for the Caribbean region which also had little meteorological activity. The method of computing satellite-derived wind fields used by Hubert and Thomasell is capable only of producing wind fields at poorly-defined altitudes in meteorologically inactive regions, while the method used in the present study is capable of producing wind fields at well-defined pressure levels in meteorologically active and inactive regions.

2) Constant-pressure charts

Constant-pressure charts are presented for the 500- and 200-mb levels for each region. Figures for each level contain three fields: 1) rawinsonde wind; 2) satellite-derived geostrophic wind; and 3) differences between satellite-derived and rawinsonde wind speeds. Differences were computed by subtracting rawinsonde values from satellite values. Isolines in each figure were drawn from exact (grid-point) values; barbs were drawn to the nearest 5 m s^{-1}.

Fields of wind at 500 and 200 mb are shown in Figs. 15 and 16, respectively, for the central United States region. At 500 mb, satellite-derived and rawinsonde wind fields have similar flow patterns with centers of large differences in wind speed. Both fields of wind show anticyclonic flow and a wind speed minimum in the southeastern portion of the region, and cyclonic flow and a wind speed maximum in the northern portion. The wind speed maximum from satellite data (approximately 45 m s^{-1}) is located northeast of the maximum from rawinsonde data (about 35 m s^{-1}). Thus, there are large positive differences between satellite-derived and rawinsonde wind speeds in this area, as shown in Fig. 17. Also, satellite-derived wind speeds are about 10 m s^{-1} larger than rawinsonde wind speeds within a confined area over northeastern Texas. The 200-mb satellite and rawinsonde wind fields (Fig. 16) show similar flow patterns with cyclonic flow in

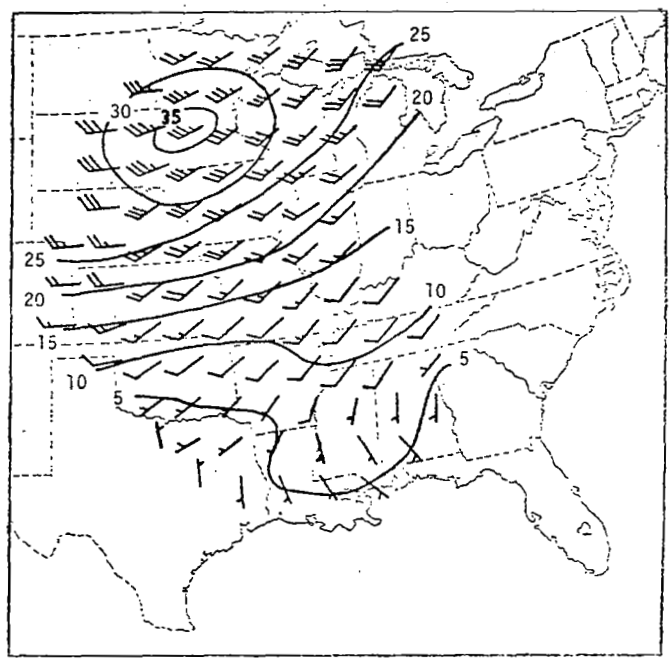

a. Rawinsonde

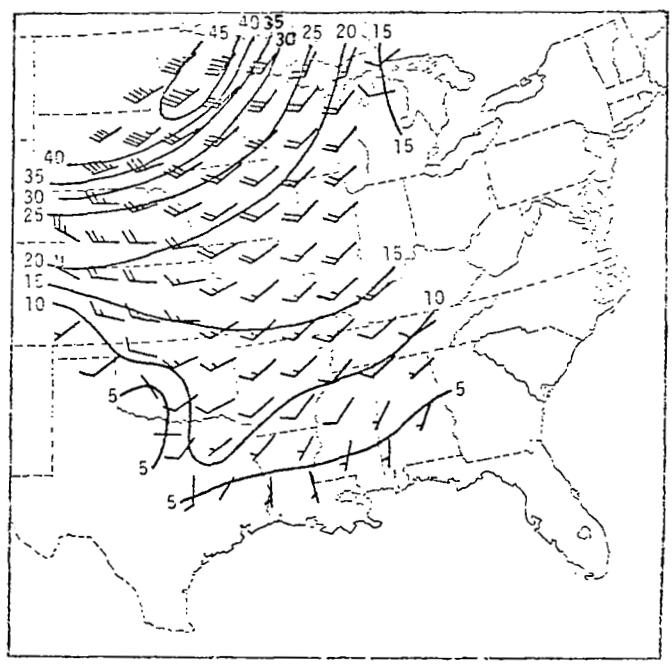

b. Satellite

Fig. 15. Plotted winds and isotach analyses (m s^{-1}) at 500 mb for the central United States region. Isotachs were drawn from exact values, barbs were plotted to nearest 5 m s^{-1}.

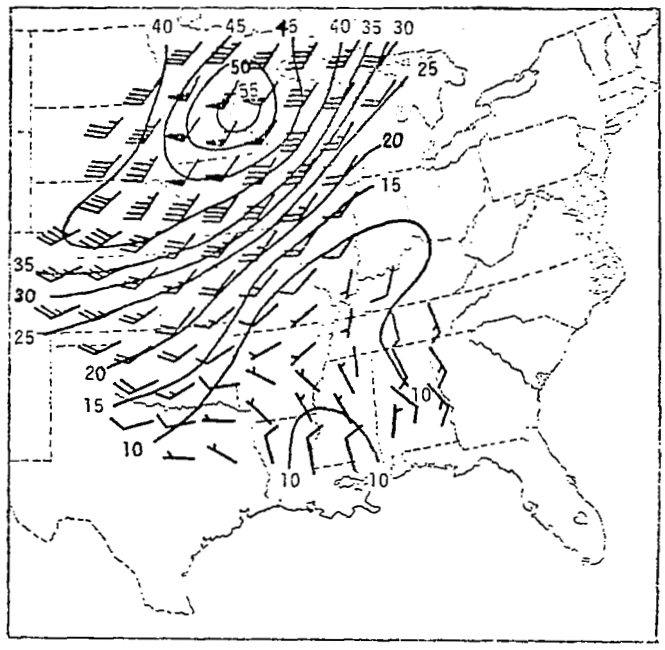

a. Rawinsonde

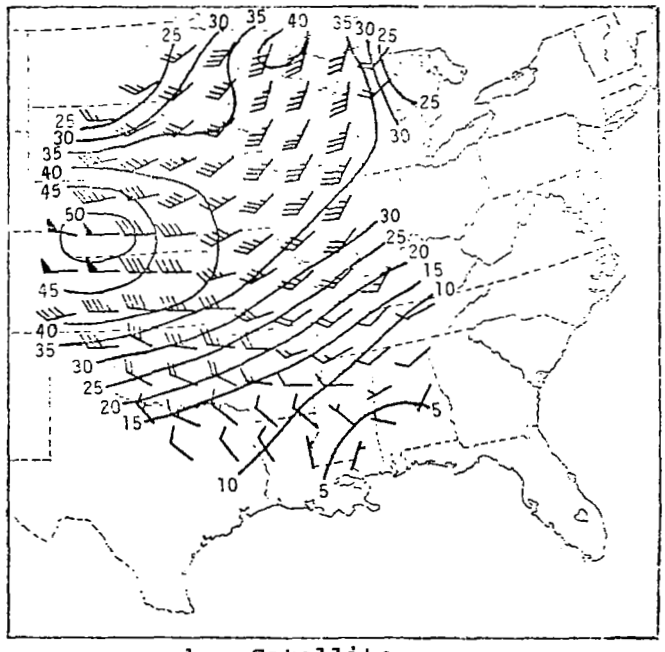

b. Satellite

Fig. 16. Plotted winds and isotach analyses (m s^{-1}) at 200 mb for the central United States region.

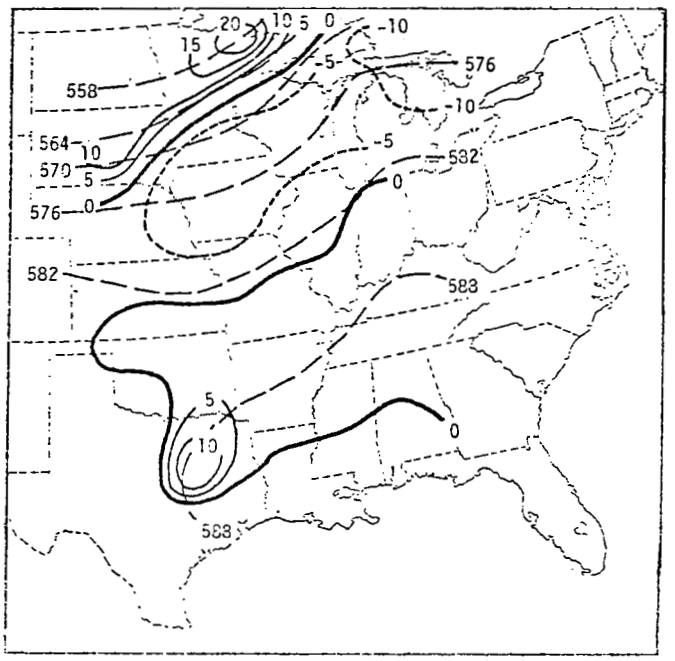

Fig. 17. Wind speed differences (m s^{-1}) (satellite minus rawinsonde values) at 500 mb for the central United States region. Superimposed on analyzed differences are satellite-derived height contours (10s of m).

the northern half of the regi n and anticyclonic flow in the southern half, but large differences in wind speed over much of the region as shown in Fig. 18. Satellite-derived wind speeds have a maximum of about 50 m s^{-1} over southern Nebraska and a second maximum of about 40 m s^{-1} over Lake Superior. The 200-mb field of rawinsonde wind shows the same axis of large wind speed but with a maximum speed of about 55 m s^{-1} over western Wisconsin. The sign of the differences between satellite-derived and rawinsonde wind speeds does not bear a relation to contour curvature. Differences in wind speeds are positive at 500 mb and negative at 200 mb over Minnesota where satellite-derived contours indicate cyclonic flow at both levels.

Satellite-derived and rawinsonde wind fields and their differences are presented here for the Caribbean region. Satellite geostrophic winds indicate more anticyclonic curvature at 500 mb than is present in the rawinsonde wind field (Fig. 19), although both fields show generally easterly winds. The differences between satellite-derived and rawinsonde wind speeds shown in Fig. 20 range from -5 to 5 m s^{-1} with the larger

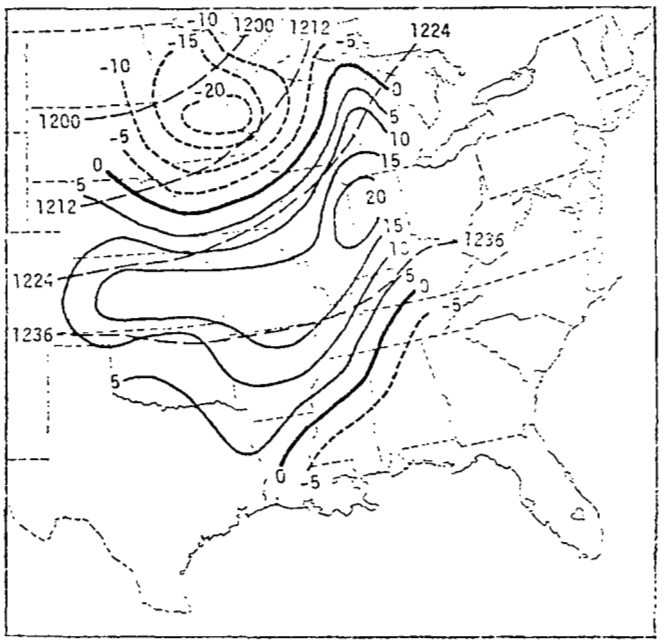

Fig. 18. Wind speed differences (m s^{-1}) (satellite minus rawinsonde values) at 200 mb for the central United States region. Superimposed on analyzed differences are satellite-derived height contours (10s of m).

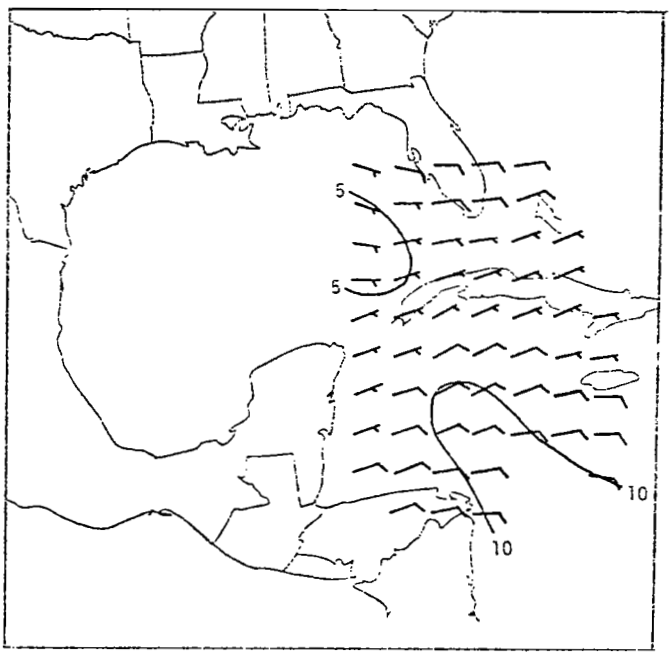

a. Rawinsonde

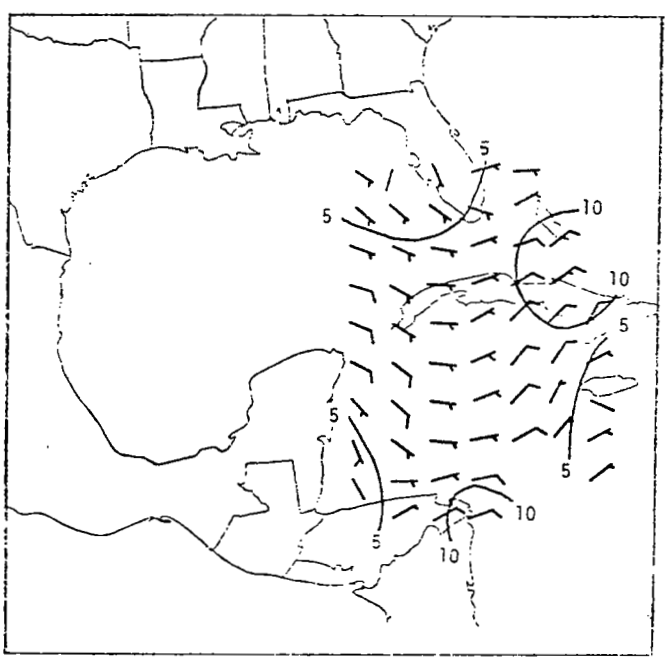

b. Satellite

Fig. 19. Plotted winds and isotach analyses (m s^{-1}) at 500 mb for the Caribbean region.

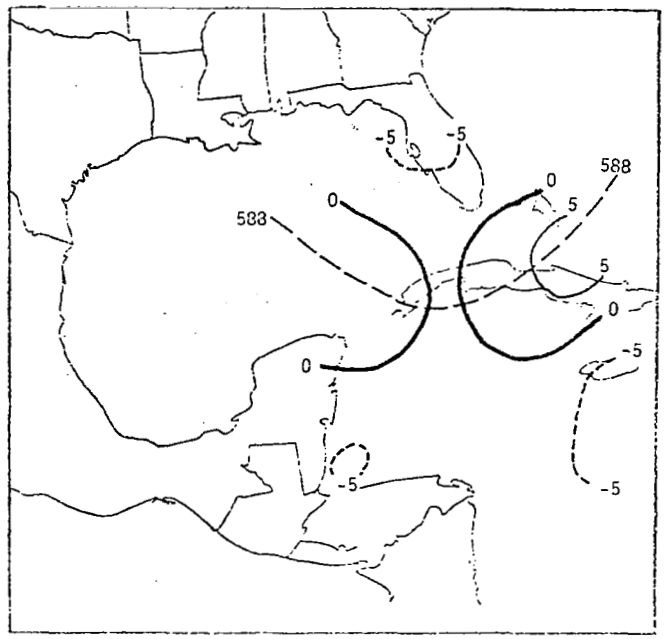

Fig. 20. Wind speed differences (m s^{-1}) (satellite minus rawinsonde values) at 500 mb for the Caribbean region. Superimposed on analyzed differences are satellite-derived height contours (10s of m).

differences confined to small areas in the region. Satellite photographs at 1630 and 1800 GMT on this day indicate extensive cloud cover over eastern Cuba; this cloud cover may be associated with large differences in wind speed in the area. The 200-mb wind fields (Fig. 21) show pronounced differences in flow patterns. The satellite-derived geostrophic wind field shows well-defined anticyclonic flow in the southern two-thirds of the region, while the rawinsonde wind field shows definite cyclonic flow. Differences between satellite-derived and rawinsonde wind patterns are greatest at this level in the Caribbean and exceed differences at any level in the other three regions. The flatness of the height field and resulting small wind speeds may be responsible for the large differences in direction; a small change in the satellite-derived height field would cause a large change in the direction of the geostrophic wind. Differences in wind speed (Fig. 22) at 200 mb range from about -5 to 10 m s^{-1} with the extreme values limited to small areas.

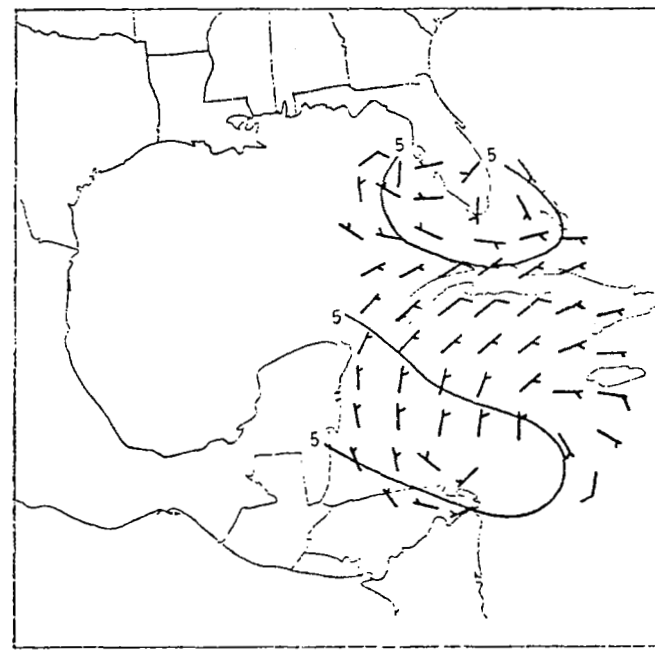

a. Rawinsonde

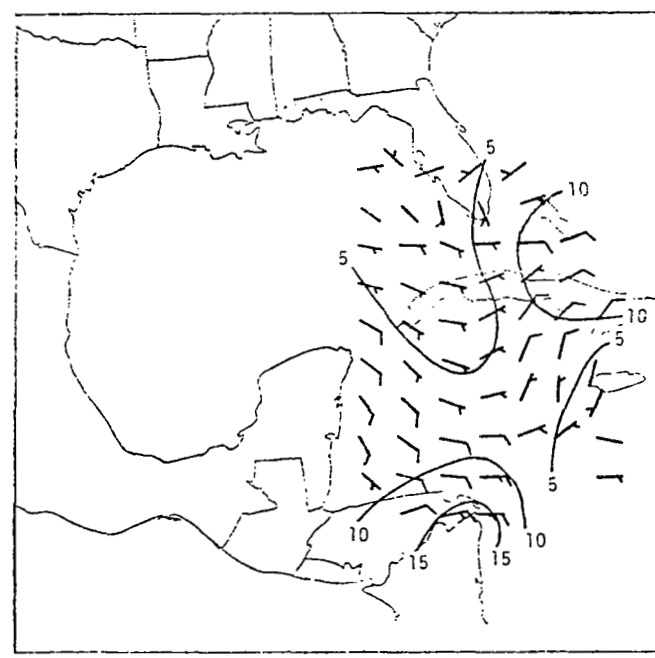

b. Satellite

Fig. 21. Plotted winds and isotach analyses (m s^{-1}) at 200 mb for the Caribbean region.

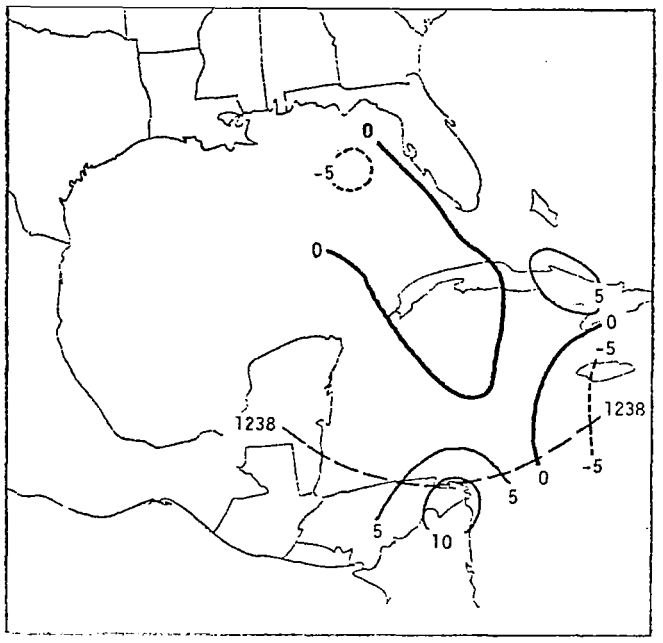

Fig. 22. Wind speed differences (m s^{-1}) (satellite minus rawinsonde values) at 200 mb for the Caribbean region. Superimposed on analyzed differences are satellite-derived height contours (10s of m).

Fields of satellite-derived and rawinsonde wind and their differences are now presented for Canada. As shown in Fig. 23, satellite-derived and rawinsonde 500-mb wind fields both show cyclonic flow over most of the region, a wind-speed maximum of about 30 m s^{-1} over Lake Superior, and a wind-speed minimum in the western part of the Canada region. Satellite-derived wind speeds at 500 mb are generally smaller than rawinsonde wind speeds with differences (Fig. 24) ranging from about -20 to 5 m s^{-1}. Satellite and rawinsonde wind fields are similar at 200 mb (Fig. 25) with generally cyclonic flow and a wind-speed maximum in the southeastern portion of the region. Differences between satellite-derived and rawinsonde wind directions are small at this level as was shown in the vertical difference profile in Fig. 11. Differences in wind speed (Fig. 26) range from near -25 to 5 m s^{-1} in the region. The field of rawinsonde wind speed has a maximum of about 60 m s^{-1} over Lake Superior, while maximum satellite wind speed is near 50 m s^{-1} and is located farther east. This leads to a maximum difference between satellite-derived and rawinsonde wind speeds of

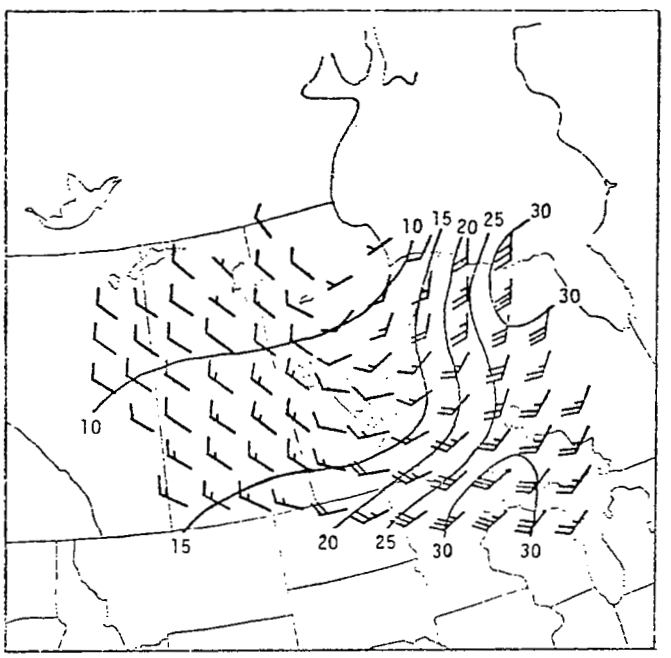

a. Rawinsonde

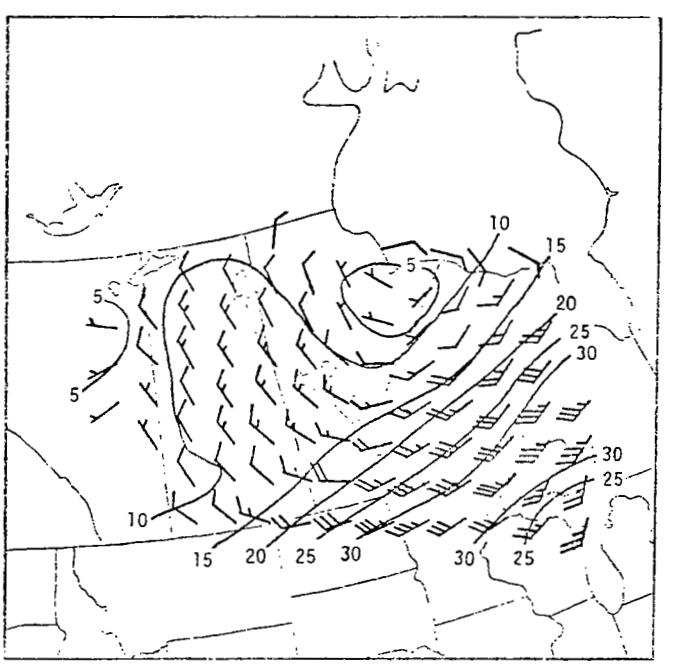

b. Satellite

Fig. 23. Plotted winds and isotach analyses (m s^{-1}) at 500 mb for the Canada region.

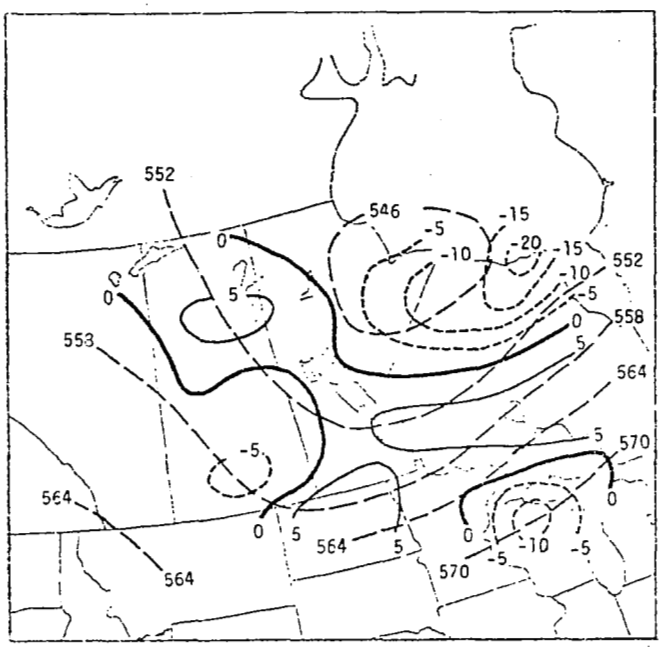

Fig. 24. Wind speed differences (m s^{-1}) (satellite minus rawinsonde values) at 500 mb for the Canada region. Superimposed on analyzed differences are satellite-derived height contours (10s of m).

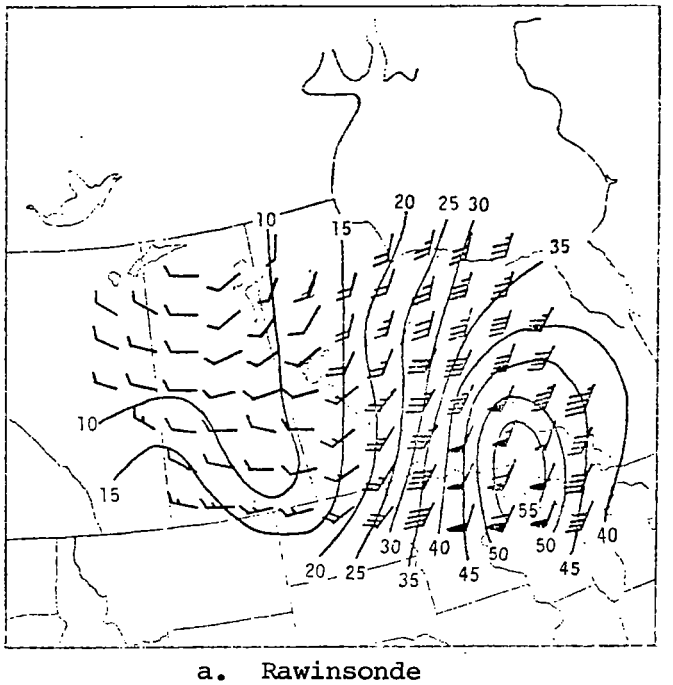

a. Rawinsonde

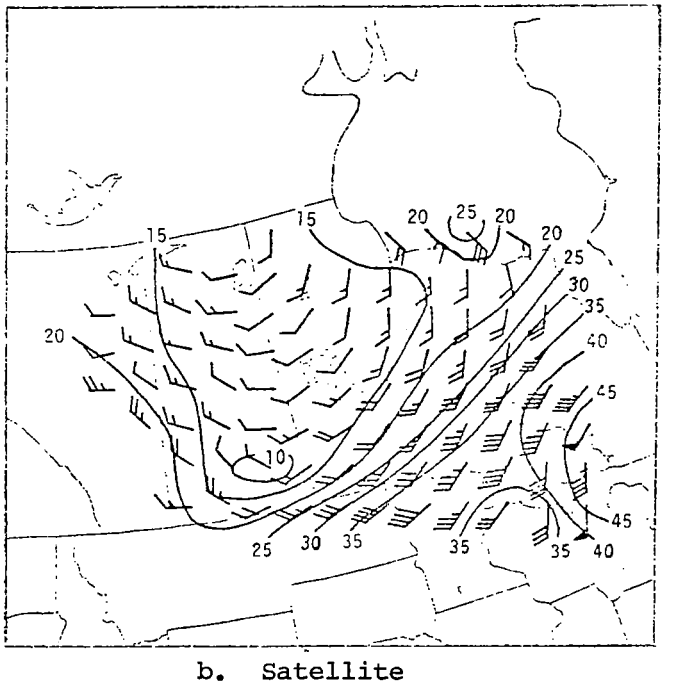

b. Satellite

Fig. 25. Plotted winds and isotach analyses (m s^{-1}) at 200 mb for the Canada region.

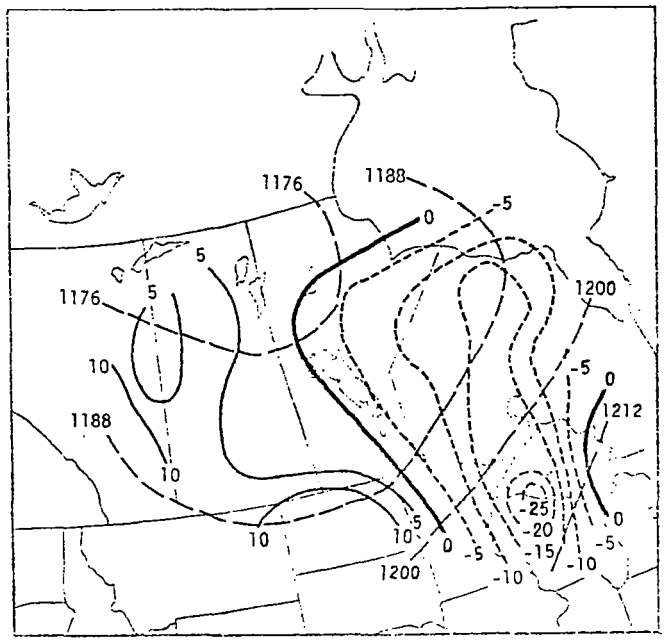

Fig. 26. Wind speed differences (m s^{-1}) (satellite minus rawinsonde values) at 200 mb for the Canada region. Superimposed on analyzed differences are satellite-derived height contours (10s of m).

about -25 m s^{-1} at the location of the rawinsonde wind-speed maximum.

Satellite-derived and rawinsonde wind fields and their differences are presented here for the western United States region. As shown in Fig. 27, both 500-mb wind fields show anticyclonic flow dominating the southeastern portion of the region and a wind-speed maximum in northwestern South Dakota. The differences in wind speed shown in Fig. 28 are near 10 m s^{-1} over southern California where the satellite-derived wind field has a second maximum of about 15 m s^{-1}. This maximum is not associated with thick clouds in the area, as was the case over Cuba. The 200-mb satellite wind field presented in Fig. 29 shows that the wind-speed maximum over southern California intensified with altitude. Magnitudes of the differences between satellite-derived and rawinsonde wind speeds (Fig. 30) are largest in this area where satellite-derived and rawinsonde wind speeds are about 50 and 10 m s^{-1}, respectively. The cause of large differences in this area is not known, but satellite data may display a phenomenon which is of short duration and, therefore,

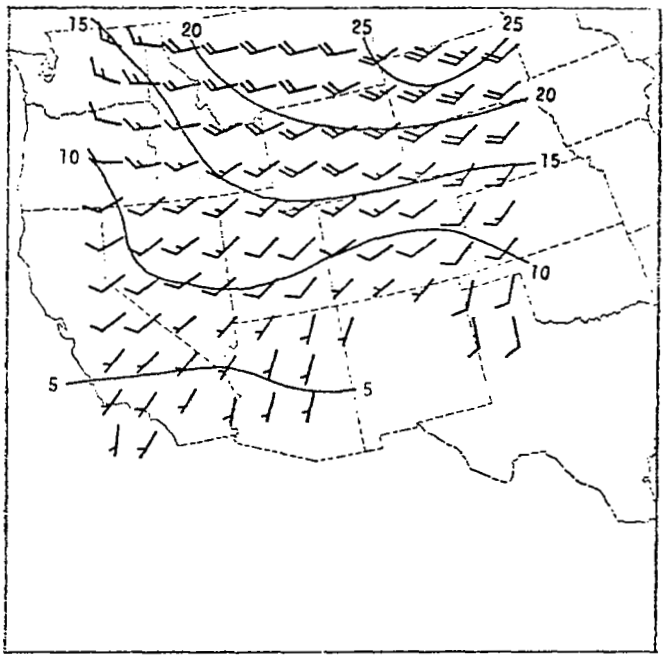

a. Rawinsonde

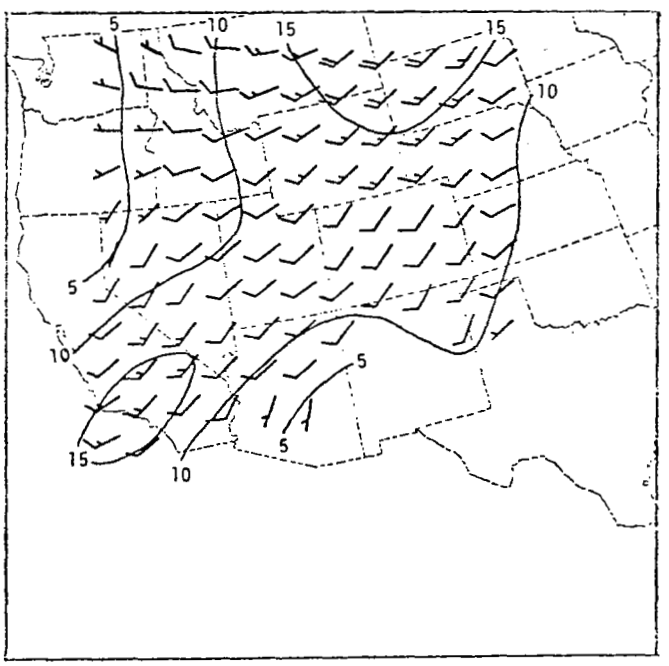

b. Satellite

Fig. 27. Plotted winds and isotach analyses (m s^{-1}) at 500 mb for the western United States region.

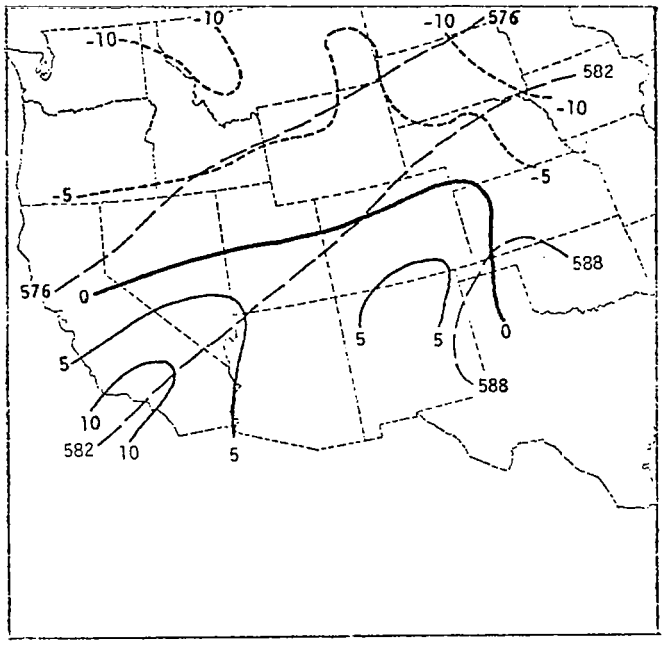

Fig. 28. Wind speed differences (m s^{-1}) (satellite minus rawinsonde values) at 500 mb for the western United States region. Superimposed on analyzed differences are satellite-derived height contours (10s of m).

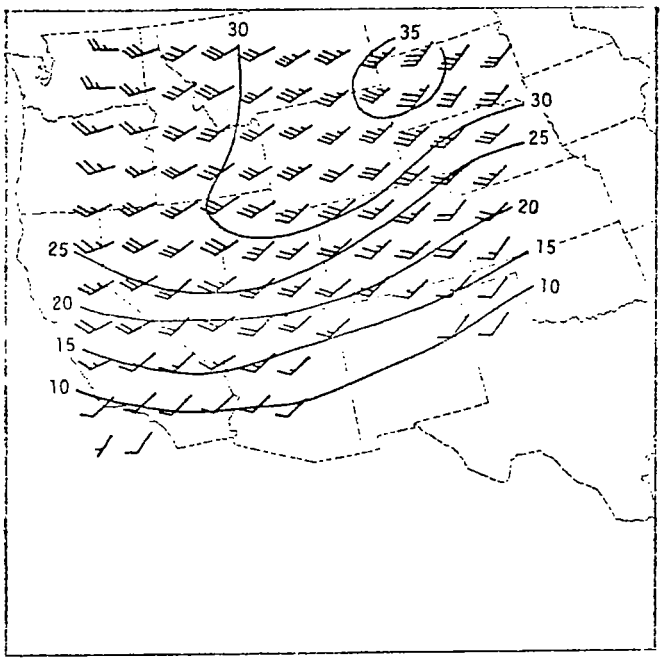

a. Rawinsonde

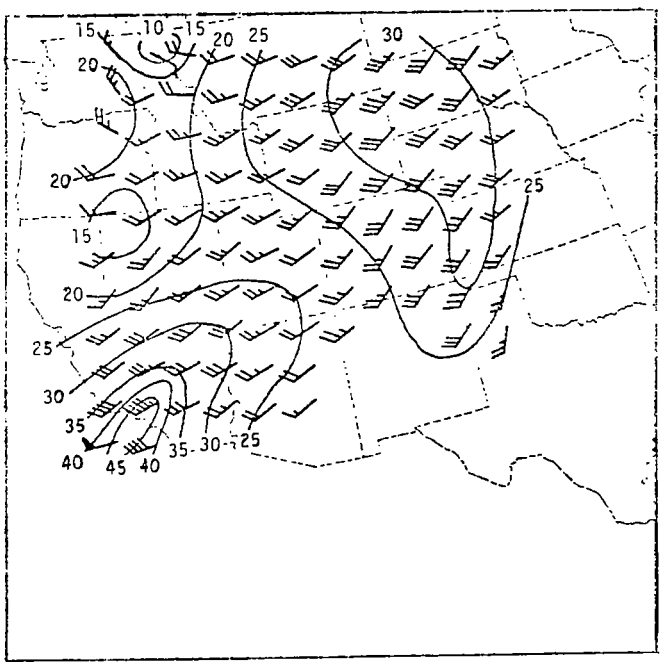

b. Satellite

Fig. 29. Plotted winds and isotach analyses (m s^{-1}) at 200 mb for the western United States region.

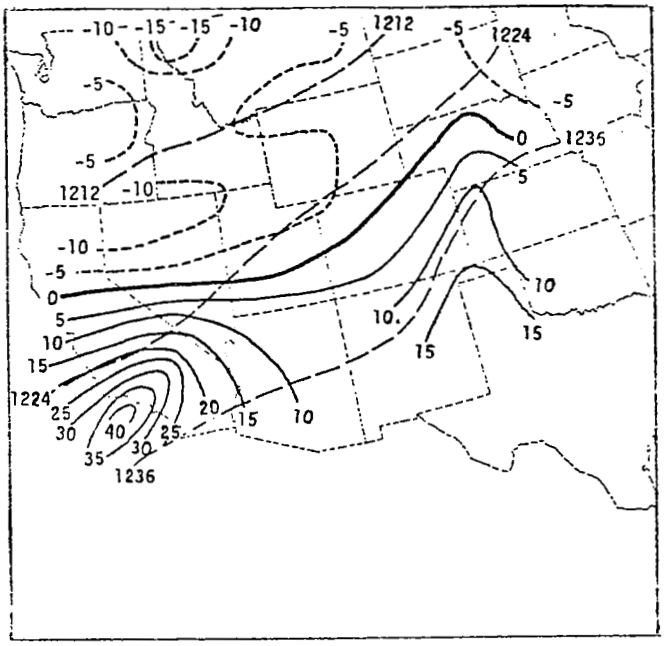

Fig. 30. Wind speed differences (m s^{-1}) (satellite minus rawinsonde values) at 200 mb for the western United States region. Superimposed on analyzed differences are satellite-derived height contours (10s of m).

is not shown in time-interpolated rawinsonde data. Maxima of geostrophic wind speeds have been found by other investigators in locations where radiosonde data show no maxima in geostrophic wind (Arnold et al., 1976). The axis of large wind speed in the satellite-derived wind field extends from southern California to western South Dakota where maximum wind speeds of about 35 m s^{-1} are indicated in satellite-derived and rawinsonde wind fields.

Petersen and Horn (1977) constructed gridded fields of 500-mb geopotential height and geostrophic wind over northeastern North America from Nimbus-6 sounding data. Satellite-derived winds obtained at 1600 GMT were compared with geostrophic winds computed from 1200 and 0000 GMT rawinsonde height analyses. Table 2 shows results for the Petersen and Horn study in the upper three rows, and for the present study in the lower four rows. Since Petersen and Horn compared satellite- and rawinsonde-derived geostrophic wind speeds at each rawinsonde time individually and the present study compares satellite-

Table 2. Comparison of results for 500-mb scalar wind speed (m s^{-1}) between Petersen and Horn (1977) and the present study.

	Nimbus-6 minus RW (12 GMT)		Nimbus-6 minus RW (00 GMT)		Nimbus-6 minus RW (avg. of 00 and 12 GMT)	
	Avg.	Std. Dev.	Avg.	Std. Dev.	Avg.	Std. Dev.
8/18/75	-1.0	3.5	-0.7	3.8	-	-
8/19/75	-0.4	3.5	-2.2	5.0	-	-
8/20/75	-0.4	3.7	-0.1	3.9	-	-
Caribbean	-	-	-	-	-0.9	3.1
Central U.S.	-	-	-	-	-0.1	5.8
Western U.S.	-	-	-	-	-1.9	5.6
Canada	-	-	-	-	-1.0	6.5

derived geostrophic and time-averaged rawinsonde wind speeds, the results can be compared only on a qualitative basis. Magnitudes of the standard deviation of differences in wind speed are generally smaller in the Petersen and Horn study, but both studies indicate that satellite-derived winds are capable of depicting the principal features observed in fields of rawinsonde wind.

3) Cross sections

Cross sections of satellite-derived and rawinsonde wind fields were constructed from grid-point values on constant-pressure surfaces and are presented for the two United States regions and the Canada region. Locations of grid points used in construction of cross sections are shown in Fig. 9. Each figure in this section contains three parts: 1) rawinsonde wind; 2) satellite-derived geostrophic wind; and 3) differences between satellite-derived and rawinsonde scalar wind speeds. As in previous sections, differences were computed by subtracting rawinsonde values from satellite values.

Cross sections of rawinsonde and satellite-derived wind fields and their differences are presented in Fig. 31 for the central United States region. The jet stream is well defined between 200 and 250 mb in the cross section from each type of data with a wind-speed maximum of about 45 m s^{-1} in the satellite data and about 50 m s^{-1} in the rawinsonde data. The jet core from rawinsonde data is located south of the jet core derived from the satellite data, as was shown in Fig. 17. This causes a difference in wind speed of about -10 m s^{-1} at the location of the rawinsonde jet core. Differences in wind speed of about 15 m s^{-1} are caused by a southward extension of the jet stream in the satellite data. Wind speeds from rawinsonde data decrease above the jet stream more rapidly than wind speeds derived from satellite data; this may be caused by vertical smoothing in satellite data. Winds from both sets of data show backing with height in the northern portion of the cross section and veering with height in the southern portion.

Cross sections of rawinsonde and satellite-derived wind fields and their differences are presented in Fig. 32 for Canada. The jet stream present in the central United States also is present between 200 and 250 mb in cross sections of rawinsonde and satellite winds in Canada. Maximum wind speeds in the cross sections of satellite-derived and rawinsonde wind fields are about 45 and 60 m s^{-1}, respectively, and the jet core is indicated near the same location in cross sections of wind from both sets of data. The satellite-derived jet stream is spread vertically with a small decrease of wind speed with height, while the rawinsonde jet stream is spread horizontally with a large decrease of wind speed above and below the jet core. The wind backs with height at each grid point in cross sections for both sets of data.

Cross sections of rawinsonde and satellite-derived wind fields and their differences are shown in Fig. 33 for the western United States. A wind speed maximum of about 35 m s^{-1} near 200 mb in the northern portion of the cross section and a horizontally-elongated axis of the jet stream are shown in cross sections from both wind fields. A second maximum in wind speed of about 30 m s^{-1} is located in the southern end of the cross section of satellite-derived wind and causes differences in wind speed of about 10 m s^{-1}. The jet core from

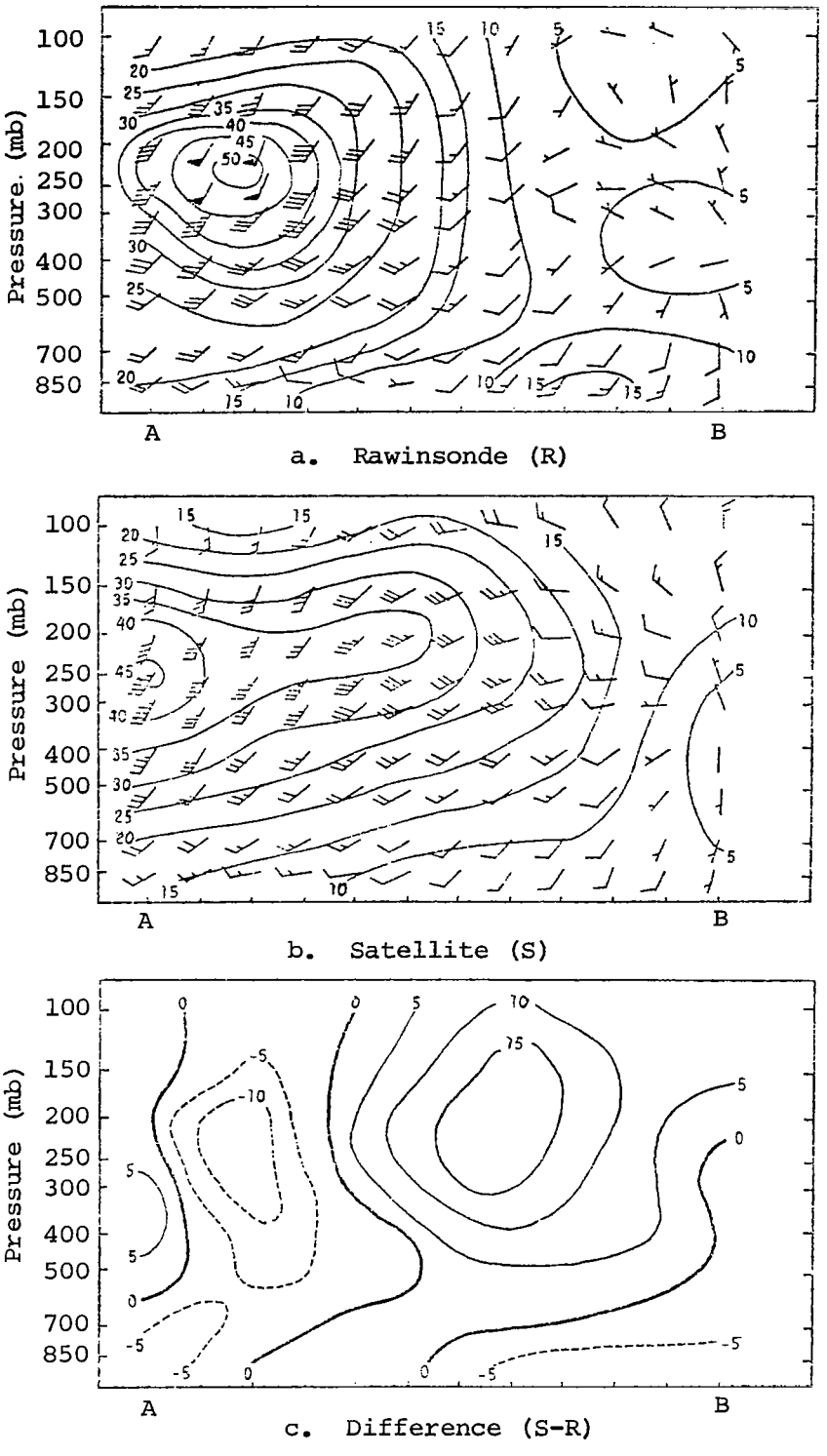

Fig. 31. Cross sections of satellite-derived and rawinsonde wind (m s^{-1}) and wind-speed differences along line AB of Fig. 9 for the central United States region.

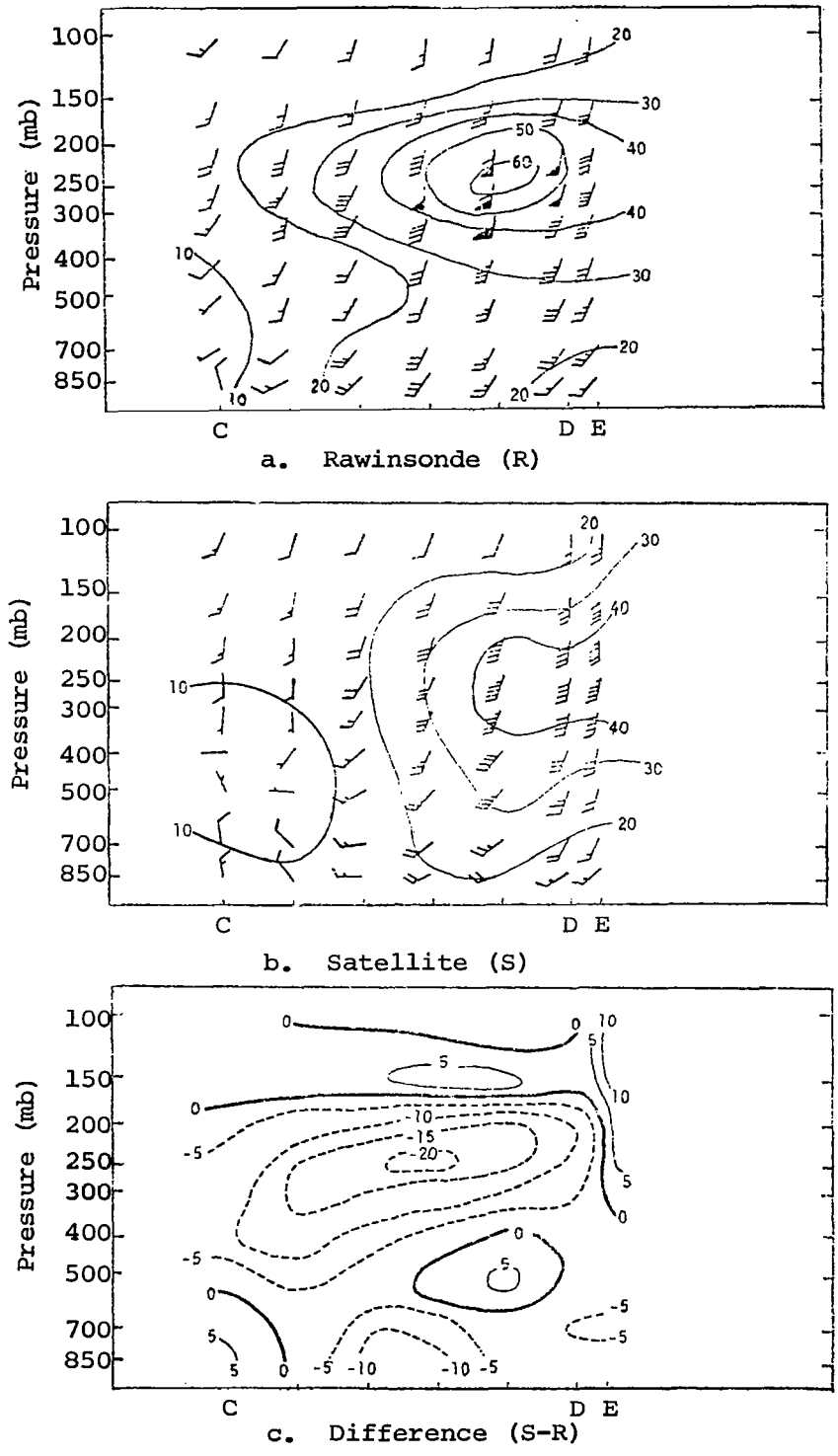

Fig. 32. Cross sections of satellite-derived and rawinsonde wind (m s^{-1}) and wind-speed differences along line CDE of Fig. 9 for the Canada region.

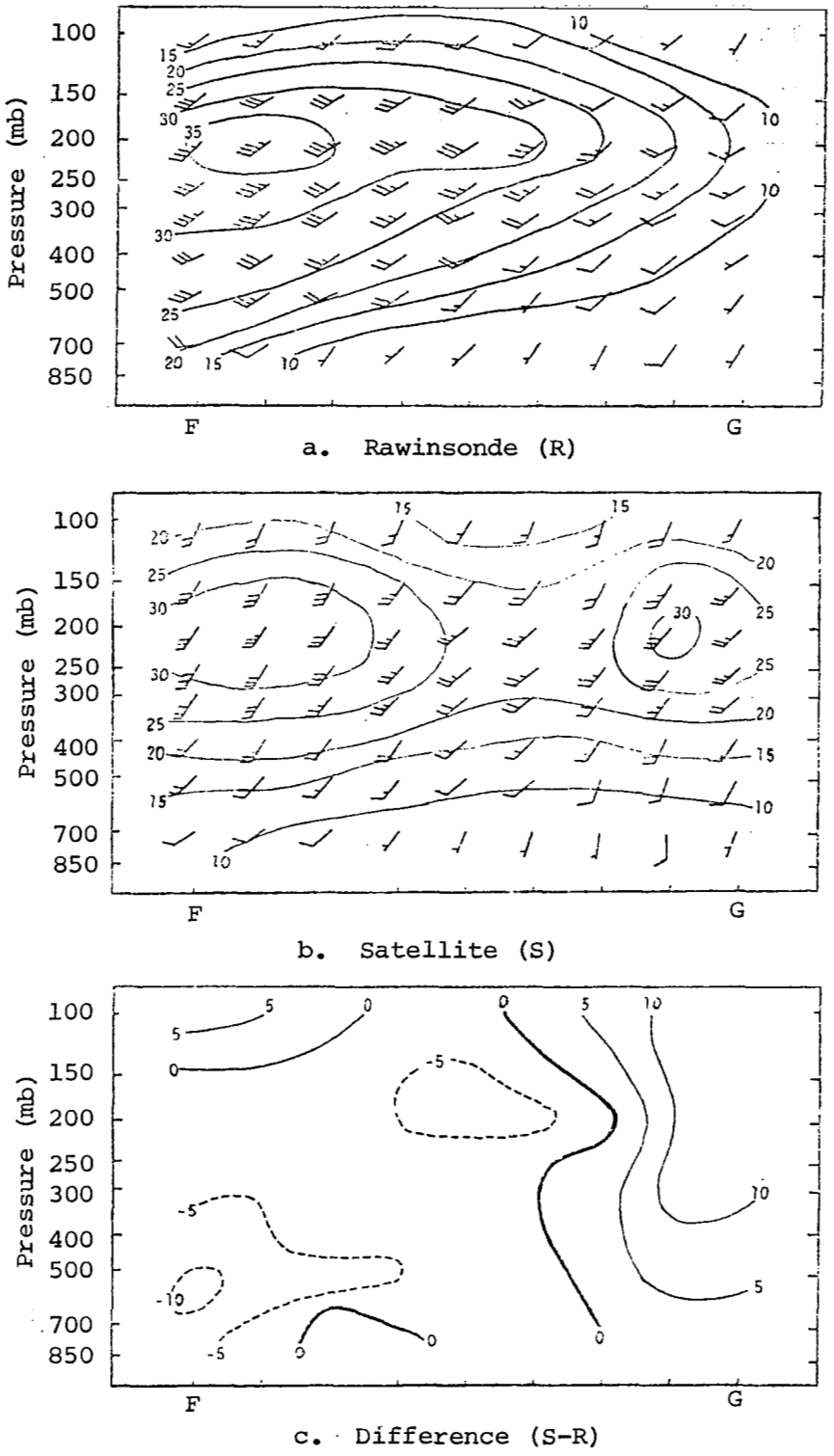

Fig. 33. Cross sections of satellite-derived and rawinsonde wind (m s^{-1}) and wind-speed differences along line FG of Fig. 9 for the western United States region.

satellite data has less vertical shear of wind speed than is present in the rawinsonde jet core. There is no significant turning of the wind with height in the cross section of wind from either type of data.

Kapela and Horn (1975) constructed isentropic cross sections using Nimbus-5 satellite sounding data. Gradient wind speeds derived from these cross sections were compared to cross sections of rawinsonde wind. The general pattern of the satellite-derived isotachs was similar to that of the rawinsonde winds but magnitudes of the maxima differed considerably. Table 3 shows the ability of the Nimbus-5 sounding data to describe the jet maximum in the Kapela and Horn study. A comparison of these results with those from the present study (shown in Table 3) indicates the Nimbus-5 and Nimbus-6 data have similar difficulty in describing the horizontal location of the jet core, but that Nimbus-6 data are superior in ability to resolve the strength and altitude of the jet core.

Table 3. Comparisons of the features of the jet core as described by rawinsonde and satellite data.

	Kapela and Horn (1975)		Present Study*	
	Rawinsonde	Nimbus-5	Rawinsonde	Nimbus-6
Latitude (N)	28	26	47	45
Altitude (mb)	270	225	230	240
Speed (m s^{-1})	70	57	50	45

* Results are for the central United States region.

b. Gradient wind

Gradient wind was computed from satellite data according to the equations presented in Sect. 5c. Satellite-derived gradient wind speed is smaller than geostrophic speed in areas of cyclonic flow and larger than geostrophic speed in areas of anticyclonic flow. This deviation from geostrophic speed is expected when centripetal acceleration is considered.

Satellite-derived gradient wind speeds compare less favorably to rawinsonde wind speeds at every pressure level than do satellite-

derived geostrophic wind speeds. Use of the gradient wind approximation decreased differences between satellite-derived and rawinsonde wind speeds at 30- to 50-percent of the grid points, and increased the standard deviation of the differences between satellite-derived and rawinsonde wind speeds at each pressure level. From the average and standard deviation of the differences between satellite-derived geostrophic and rawinsonde wind speeds at each pressure level, vertical averages were obtained which encompass all pressure levels for three of the regions studied. These vertical averages are presented in the first two columns of Table 4. The second two columns of this table present the corresponding quantities for the satellite-derived gradient wind. The table shows that the average standard deviation of the differences between satellite-derived and rawinsonde wind speeds was increased in all three regions by the use of the gradient wind approximation, while the magnitude of the average difference was decreased in two of the three regions.

Table 4. Vertically-averaged differences and standard deviations of the differences (m s^{-1}) between satellite-derived and rawinsonde wind speeds.

	Geostrophic - Rawinsonde		Gradient - Rawinsonde	
Region	Avg.	Std. Dev.	Avg.	Std. Dev.
Central United States	1.9	7.7	-0.7	8.8
Canada	-0.8	8.6	-2.7	9.1
Western United States	0.9	8.6	0.5	8.8

The gradient wind approximation did not improve comparisons between satellite-derived and rawinsonde wind speeds. This is because the differences between satellite geostrophic and rawinsonde wind speeds do not correspond to the curvature of the satellite-derived contours. Areas of large positive and negative differences between satellite-derived geostrophic and rawinsonde wind speeds are not associated with troughs, ridges, or any other large-scale pattern. This is evident in the difference fields in Figs. 17, 18, 20, 22, 24, 26, 28,

and 30. The lack of correspondence between satellite-derived contours and differences between satellite geostrophic and rawinsonde wind speeds may be caused by the time interpolation of rawinsonde winds in this study. Kapela and Horn (1975) found that use of the gradient wind approximation decreased differences between satellite-derived and rawinsonde wind speeds when they compared 1630 GMT Nimbus-5 with 1200 GMT rawinsonde data.

c. Surface wind

Surface wind was computed from satellite data according to the equation presented in Sect. 5d. Average differences and standard deviations of the differences between satellite-derived and hourly-observed surface winds are presented in Table 5 for the central United States, Caribbean, and Canada regions. Fields of surface wind were not computed in the western United States region because of large variability of terrain height. The average difference and the standard

Table 5. Average differences and standard deviations of the differences between satellite-derived (S) and hourly-observed (O) surface winds (S-O) for the three regions.

	Speed ($m\ s^{-1}$)		Direction (deg)	
	Avg.	Std. Dev.	Avg.	Std. Dev.
Central United States	-0.3	2.1	16	34
Caribbean	1.5	2.8	21	66
Canada	0.9	4.3	30	28

deviation of differences between satellite-derived and observed surface wind speeds are smallest in the central United States region where observed wind speeds were generally between 3 and 8 $m\ s^{-1}$. The large standard deviation of the differences in wind speed in Canada may be associated with the large wind speeds and the intense low-pressure center in the region. The average and standard deviation of the differences between satellite-derived and observed wind speeds in the Caribbean are larger than expected in this region of very low wind speeds.

The magnitude of the standard deviation of the differences between satellite-derived and observed wind directions is largest in the Caribbean region where surface winds were light and variable. The magnitude of the standard deviation of the differences in surface wind direction is smallest in Canada where the satellite-derived flow pattern is very similar to the well-organized observed flow pattern.

Fields of satellite-derived and observed surface winds and their differences are presented for the central United States. Both fields of wind shown in Fig. 34 indicate anticyclonic flow in the southeastern portion of the region, weak cyclonic flow in the northern portion, and strong cyclonic flow around the surface low-pressure center in Oklahoma. Differences between satellite-derived and observed wind speeds (Fig. 35) range from about -5 to 5 m s^{-1} but have magnitudes less than 2.5 m s^{-1} at most grid points. Observed surface winds accelerate as they cross the isobars toward lower pressure. This acceleration was not taken into account in the computation of satellite-derived surface wind speeds and leads to negative differences in wind speed (satellite-derived speeds are too small) near Oklahoma and the Great Lakes.

Fields of satellite-derived and observed surface winds and their differences are presented for the Caribbean region. As shown in Fig. 36, there are significant differences between observed and satellite-derived flow patterns. Observed winds indicate anticyclonic flow in the northern half of the region and cyclonic flow in the southern half, while satellite-derived surface winds indicate anticyclonic flow in the eastern half of the region and cyclonic flow in the western half. These differences between satellite-derived and observed surface wind directions may be caused by the small magnitudes of observed wind speed in the region. Differences in wind speed shown in Fig. 37 are generally positive in the region and range from about -3 to 5 m s^{-1}.

Fields of satellite-derived and observed surface winds and their differences are presented for Canada. As shown in Fig. 38, the two wind fields have similar flow patterns (they both show cyclonic flow in most of the region) but contain large differences in wind speed.

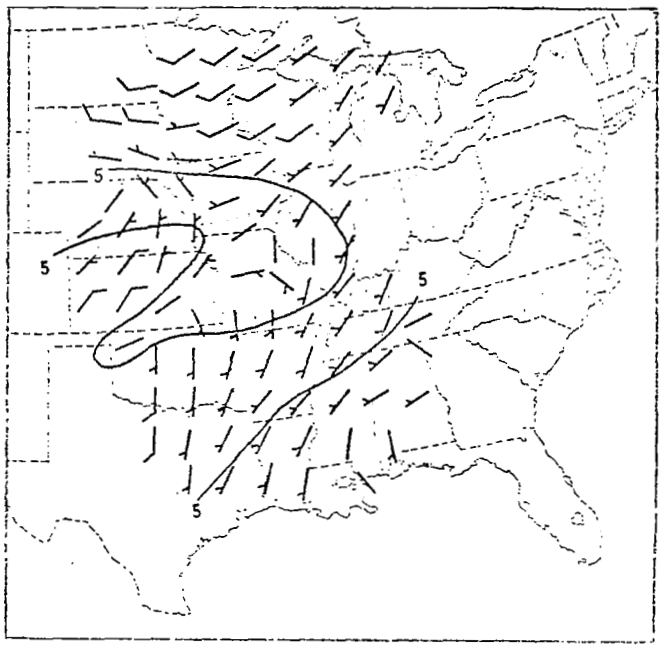

a. Observed

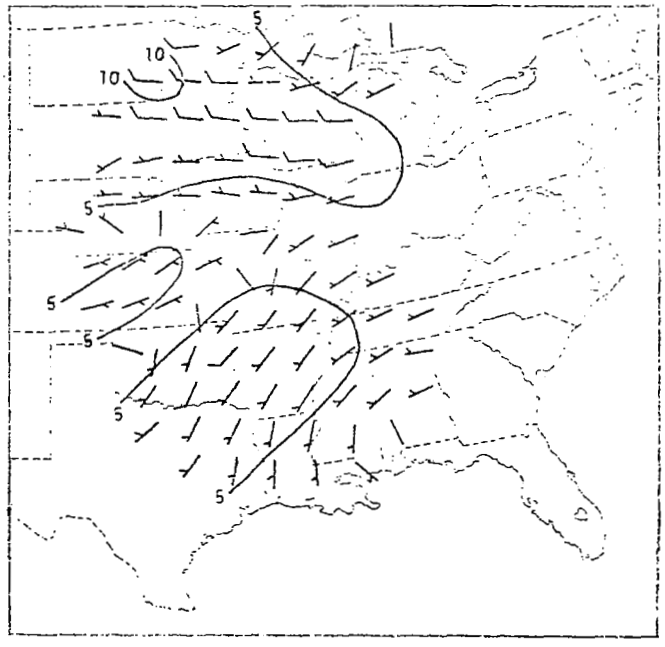

b. Satellite

Fig. 34. Plotted surface wind and isotach analyses (m s^{-1}) for the central United States region.

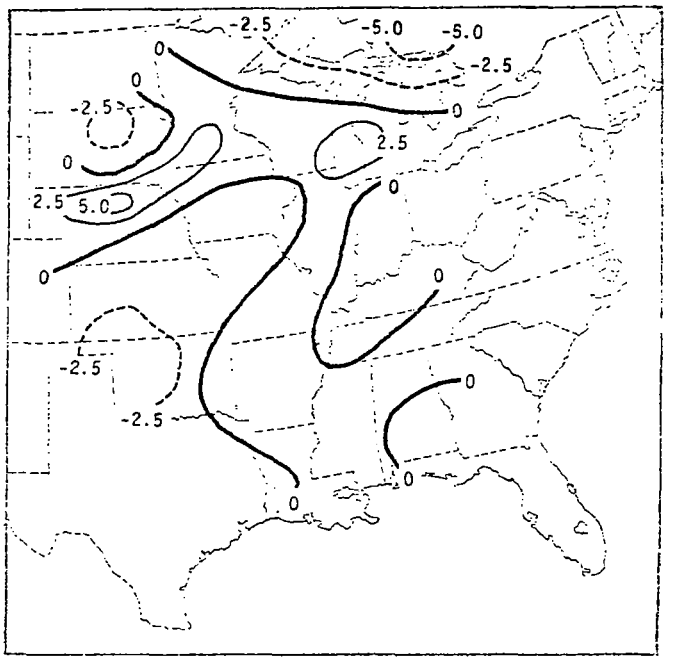

Fig. 35. Surface wind speed differences (m s^{-1}) (satellite minus observed values) for the central United States region. An interval of 2.5 m s^{-1} was used for the analysis of wind speed differences.

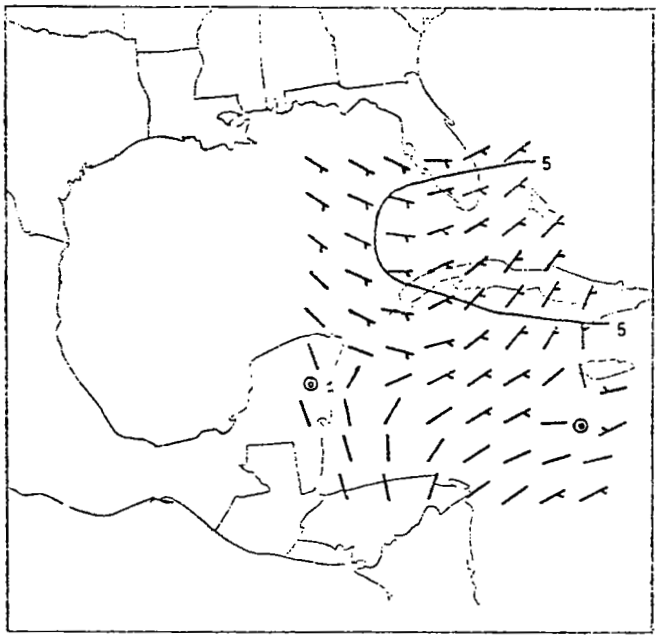

a. Observed

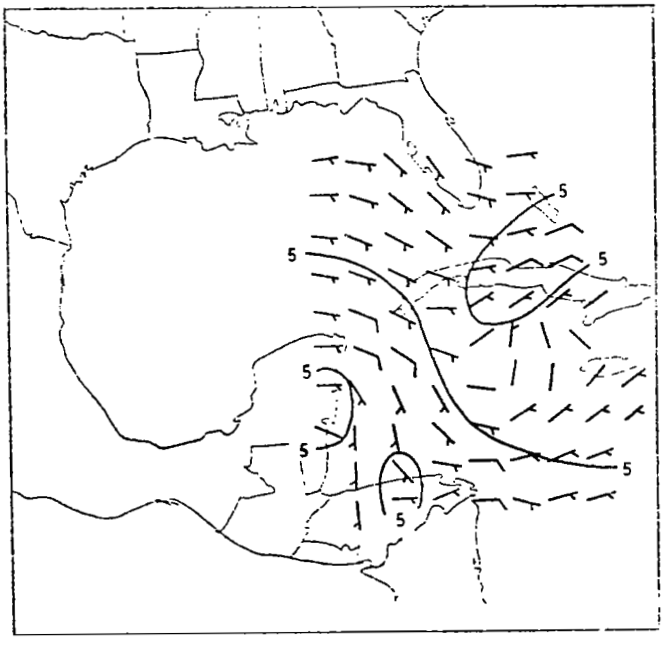

b. Satellite

Fig. 36. Plotted surface wind and isotach analyses (m s^{-1}) for the Caribbean region.

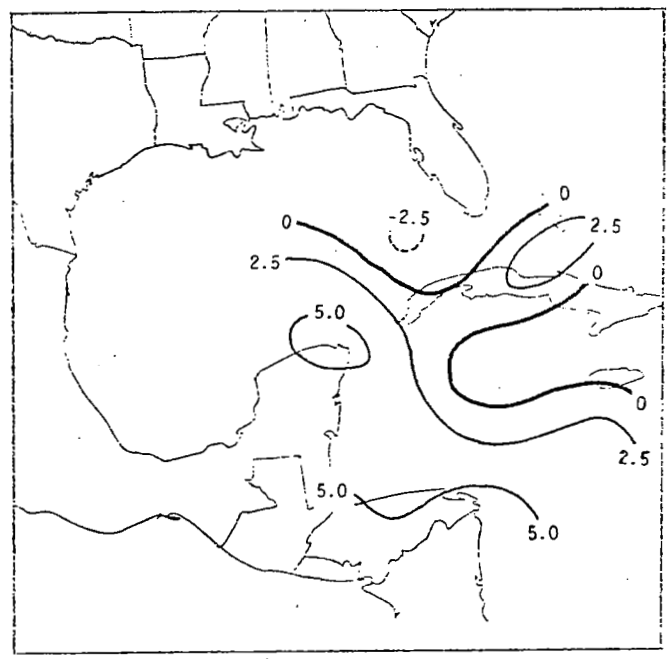

Fig. 37. Surface wind speed differences (m s^{-1}) (satellite minus observed values) for the Caribbean region. An interval of 2.5 m s^{-1} was used for the analysis of wind-speed differences.

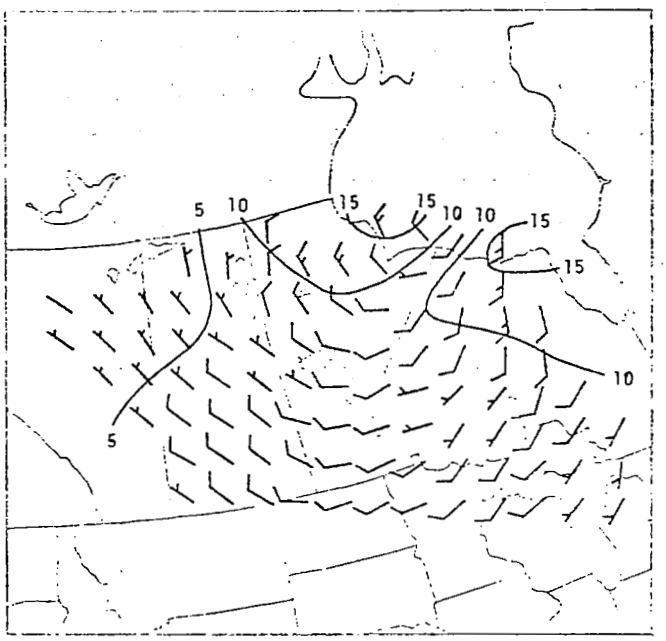

a. Observed

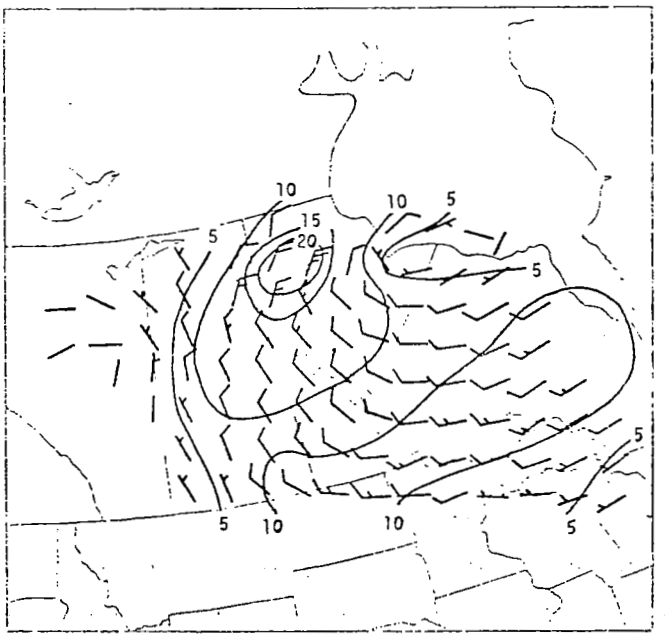

b. Satellite

Fig. 38. Plotted surface wind and isotach analyses (m s^{-1}) for the Canada region.

Satellite-derived surface winds indicate closed circulation with small wind speeds near the low-pressure center south of Hudson Bay, while observed winds cross the isobars toward lower pressure and have larger speeds than the satellite-derived winds. Except near the low-pressure center, differences between satellite-derived and observed surface wind speeds (Fig. 39) are generally positive (satellite-derived speeds are too large). It is not known why the satellite-derived wind speed is about 10 m s^{-1} larger than observed wind speed southwest of Hudson Bay.

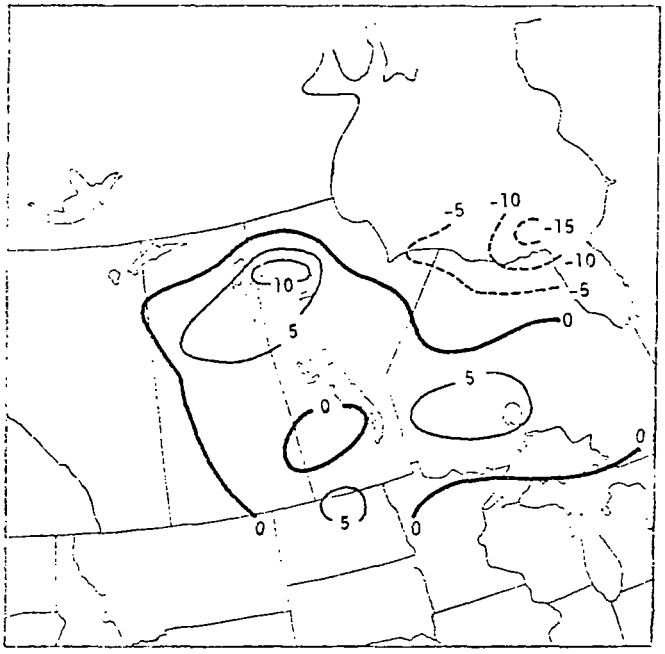

Fig. 39. Surface wind speed differences (m s^{-1}) (satellite minus observed values) for the Canada region.

d. Kinematic parameters

Fields of horizontal advection of temperature at 850 and 500 mb are presented in Figs. 40 and 41, respectively, for the central United States. At 850 mb, rawinsonde and satellite-derived fields of temperature advection indicate cold-air advection over northern Wisconsin and warm-air advection over northeastern Oklahoma. Magnitudes of warm-air advection are very nearly the same for both types of data, while satellite-derived magnitudes of cold-air advection over Wisconsin

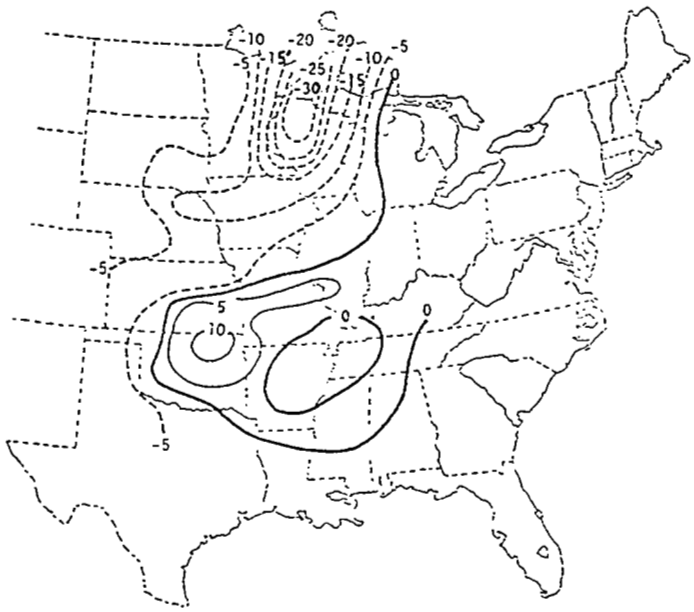

a. Rawinsonde

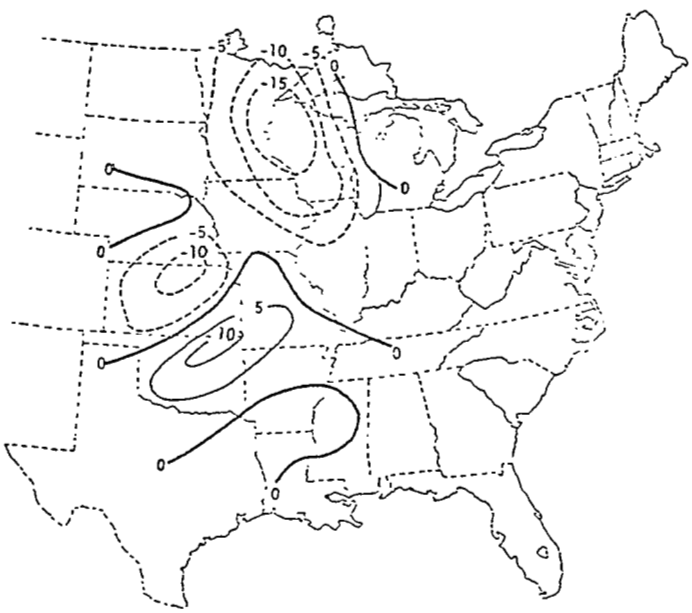

b. Satellite

Fig. 40. Fields of horizontal advection of temperature (10^{-5} °C s^{-1}) at 850 mb for the central United States region.

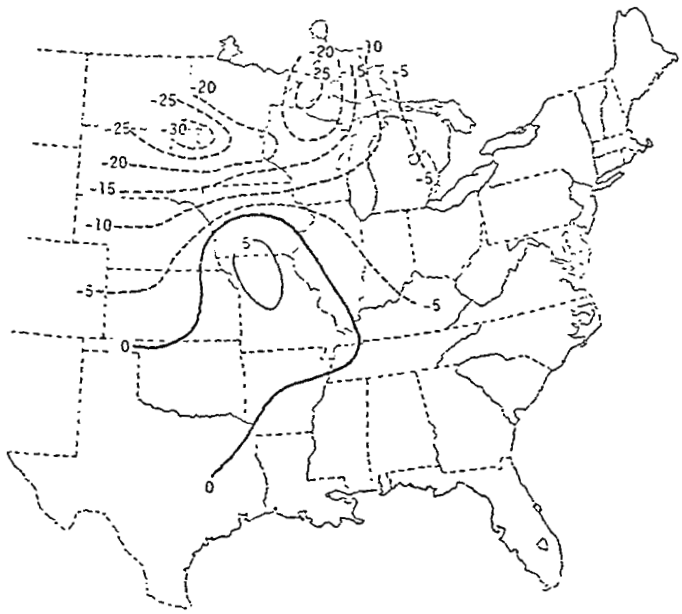

a. Rawinsonde

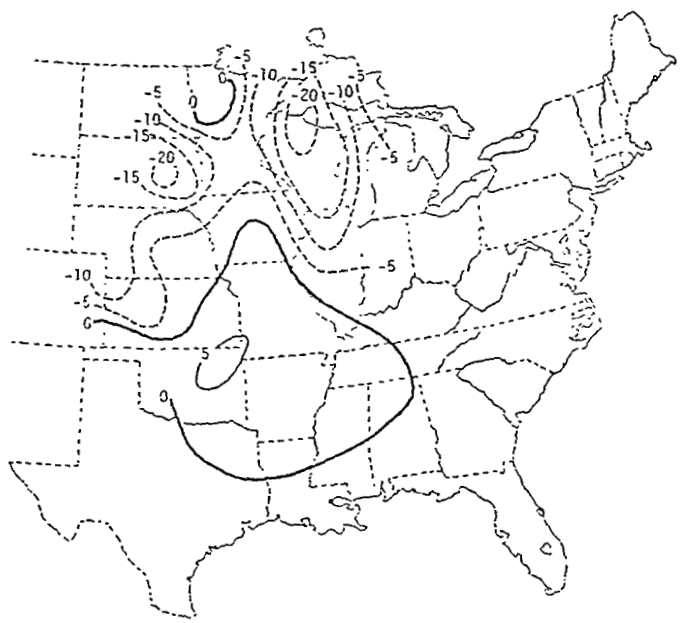

b. Satellite

Fig. 41. Fields of horizontal advection of temperature (10^{-5} °C s^{-1}) at 500 mb for the central United States region.

are smaller than the rawinsonde values. At 500 mb, fields of temperature advection from both types of data show cold-air advection centered over northern Wisconsin and eastern South Dakota; magnitudes of satellite-derived cold-air advection are smaller than rawinsonde values in both locations. Centers of maximum warm-air advection computed from the two types of data do not coincide but occur in the same general area with approximately the same magnitudes. Fields of horizontal advection of temperature for the other three regions (not shown) indicate that satellite data are capable of depicting centers of positive and negative temperature advection for each of the synoptic conditions considered in this study.

Fields of the vertical component of relative vorticity at 500 mb are presented in Fig. 42 for the central United States region. There is little correspondence between the rawinsonde and satellite-derived fields of vorticity. Centers of relative vorticity from the two sets of data are generally of opposite sign. Correspondence between rawinsonde and satellite-derived fields of relative vorticity is no better in the Caribbean and western United States regions. Fields of relative vorticity computed from the two types of data are similar only in Canada where the 500-mb flow was strong and cyclonic.

The field of satellite-derived advection of absolute vorticity at 500 mb (not shown) is dissimilar to the corresponding rawinsonde field in each of the four regions. The dissimilarity is expected since the advection of vorticity involves the second derivative of rawinsonde and satellite-derived wind components which are significantly different (as shown in Figs. 12 and 13).

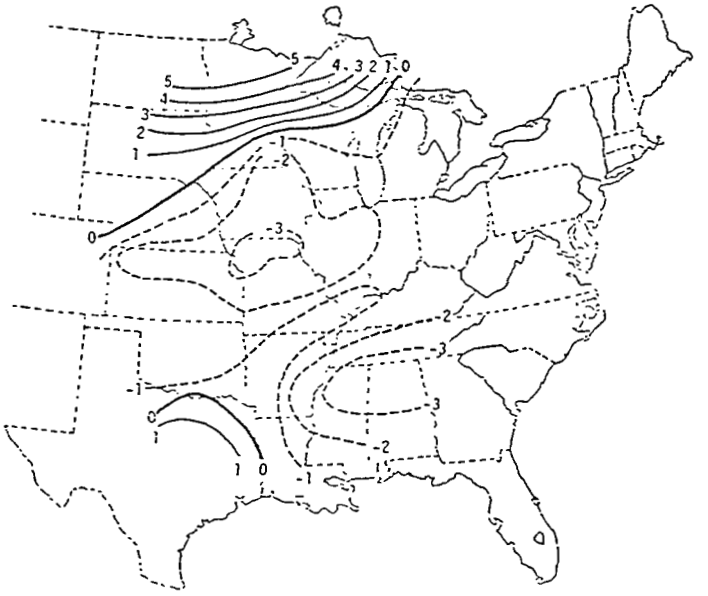

a. Rawinsonde

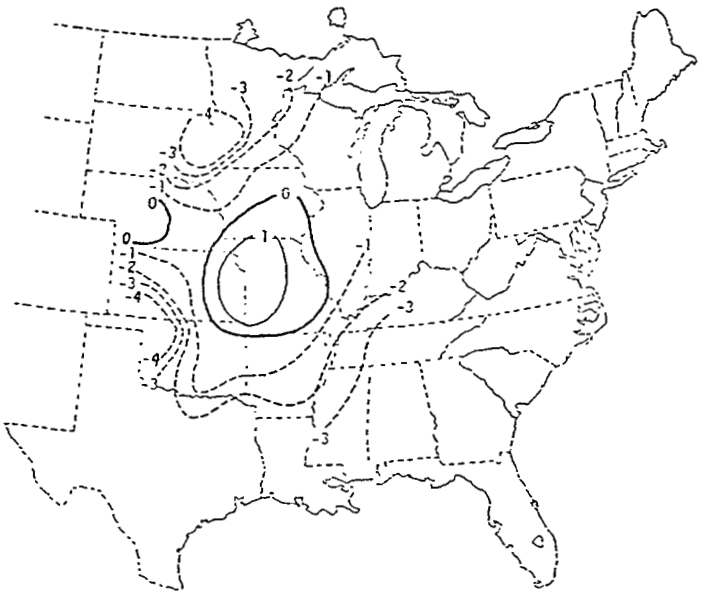

b. Satellite

Fig. 42. Fields of the vertical component of relative vorticity ($10^{-5}s^{-1}$) at 500 mb for the central United States region.

7. SUMMARY AND CONCLUSIONS

a. Summary

Objective methods of computing upper-level and surface wind fields from Nimbus-6 satellite thermodynamic data were developed. Satellite-derived and rawinsonde wind fields were compared on gridded constant-pressure charts at nine pressure levels in four geographical regions. Rawinsonde winds used in the comparisons were linearly interpolated to correspond in time to the satellite pass. Fields of satellite-derived surface wind were compared to fields of hourly-observed surface wind in three regions. Finally, rawinsonde and satellite-derived kinematic parameters were compared.

b. Conclusions

The following conclusions were reached from this study:

1) The best satellite-derived wind on constant-pressure charts is a geostrophic wind derived from highly smoothed fields of geopotential height. Use of the gradient wind approximation did not improve comparisons between satellite-derived and rawinsonde winds.

2) Circulation patterns from satellite-derived geostrophic and rawinsonde wind fields are similar in regions of moderate to large wind speeds, but may compare poorly in regions of small wind speeds.

3) Mean differences between satellite-derived geostrophic and rawinsonde wind speeds range from about -5 to 5 m s^{-1}. Magnitudes of the standard deviation of the differences in wind speed range from about 3 to 12 m s^{-1} on constant-pressure surfaces and peak at the jet-stream level.

4) Centers of maximum wind speed in satellite-derived wind fields may be displaced horizontally from the corresponding centers in rawinsonde data; a second maximum in wind speed may be present in satellite-derived winds where none exists in rawinsonde data. Satellite-derived and rawinsonde winds show good agreement on the altitude of the jet stream core, but the jet core from satellite data has smaller wind speeds and less vertical shear of wind than are present in the rawinsonde jet core.

5) Fields of satellite-derived surface wind computed with the logarithmic wind law agree well with fields of observed surface wind in most regions. Satellite-derived surface winds are able to depict flow across a cold front and around a low-pressure center. Magnitudes of the standard deviation of the differences in surface wind speed range from about 2 to 4 m s^{-1}, while magnitudes of the standard deviation of the differences in wind direction range from about 28 to 66°.

6) Rawinsonde and satellite-derived fields of temperature advection are similar at 850 and 500 mb. However, there is little correspondence between rawinsonde and satellite-derived fields of vorticity or vorticity advection at 500 mb.

REFERENCES

Arnason, G., G. J. Haltiner, and M. J. Frawley, 1962: Higher-order geostrophic wind approximations. Mon. Wea. Rev., 90, 175-185.

Arnold, J. E., J. R. Scoggins, and H. E. Fuelberg, 1976: A comparison between Nimbus-5 THIR and ITPR temperatures and derived winds with rawinsonde data obtained in the AVE II experiment. NASA Contractor Report CR-2757, 76 pp.

Barnes, S. L., 1964: A technique for maximizing detail in numerical weather map analysis. J. Appl. Meteor., 3, 396-409.

Fiedler, F., and H. A. Panofsky, 1972: The geostrophic drag coefficient and the effective roughness length. Quart. J. Roy. Meteor. Soc., 98, 213-220.

Garratt, J. R., 1977: Review of drag coefficients over oceans and continents. Mon. Wea. Rev., 105, 915-929.

Hess, S. L., 1959: Introduction to Theoretical Meteorology. New York, Holt, Rinehart, and Winston, 362 pp.

Horn, L. H., R. A. Petersen, and T. M. Whittaker, 1976: Intercomparisons of data derived from Nimbus 5 temperature profiles, rawinsonde observations and initialized LFM model fields. Mon. Wea. Rev., 104, 1363-1371.

Hubert, L. F., and Thomasell, A., 1979: Error characteristics of satellite-derived winds. NOAA Technical Report NESS 79, 35 pp.

_____, and L. F. Whitney, 1971: Wind estimates from geostationary-satellite pictures. Mon. Wea. Rev., 99, 665-672.

Kapela, A. F., and L. H. Horn, 1975: Nimbus-5 satellite soundings in a strongly baroclinic region. Meteorological Applications of Satellite Indirect Soundings, Project Report, NOAA Grant 04-4-158-2, Department of Meteorology, University of Wisconsin, Madison, 1-19.

Moyer, V., J. R. Scoggins, N. M. Chou, and G. S. Wilson, 1978: Atmospheric structure deduced from routine Nimbus 6 satellite data. Mon. Wea. Rev., 106, 1340-1352.

National Weather Service, 1971: New initialization procedure for the 6-layer (PE) numerical prediction model. Technical Procedures Bulletin No. 65, 5 pp.

Petersen, R. A., and L. H. Horn, 1977: An evaluation of 500 mb height geostrophic wind fields derived from Nimbus-6 soundings. Bull. Am. Meteorol. Soc., 58, 1195-1201.

REFERENCES (Continued)

Shuman, F. G., 1957: Numerical methods in weather prediction: II Smoothing and filtering. Mon. Wea. Rev., 85, 357-361.

Smith, W. L., and H. M. Woolf, 1974: An intercomparison of meteorological parameters derived from radiosonde and satellite vertical temperature cross sections. NOAA Technical Report NESS 71, 13 pp.

_____, _____, and H. E. Fleming, 1972: Retrieval of atmospheric temperature profiles from satellite measurements for dynamical forecasting. J. Appl. Meteor., 11, 113-122.

_____, _____, C. M. Hayden, and W. C. Shen, 1975: Nimbus-5 sounding data processing system part II: Results. Final Report, NASA Contract S-70249-A6, 35 pp.

Suchman, D., and D. W. Martin, 1976: Wind sets from SMS images: An assessment of quality for GATE. J. Appl. Meteor., 15, 1265-1278.

Thomasell, A., 1979: Wind analysis by conditional relaxation. NOAA Technical Report NESS 77, 23 pp.

1. REPORT NO.	2. GOVERNMENT ACCESSION NO.	3. RECIPIENT'S CATALOG NO.
NASA RP-1072		

4. TITLE AND SUBTITLE	5. REPORT DATE
Determination of Wind from Nimbus 6 Satellite Sounding Data	January 1981
	6. PERFORMING ORGANIZATION CODE
7. AUTHOR(S)	8. PERFORMING ORGANIZATION REPORT #
William E. Carle and James R. Scoggins	
9. PERFORMING ORGANIZATION NAME AND ADDRESS	10. WORK UNIT NO.
Department of Meteorology Texas A&M University College Station, Texas 77843	M-329
	11. CONTRACT OR GRANT NO.
	13. TYPE OF REPORT & PERIOD COVERED
12. SPONSORING AGENCY NAME AND ADDRESS	Reference Publication
U.S. Army Research Office Research Triangle Park, North Carolina	14. SPONSORING AGENCY CODE

15. SUPPLEMENTARY NOTES

The U. S. Army Research Office has granted permission for NASA to publish these data for use in studies using space technology for weather-related programs.

16. ABSTRACT

Objective methods of computing upper-level and surface wind fields from Nimbus-6 satellite sounding data are developed. These methods are evaluated by comparing satellite-derived and rawinsonde wind fields on gridded constant-pressure charts in four geographical regions. Satellite-derived and hourly observed surface wind fields are compared.

Results indicate that the best satellite-derived wind on constant-pressure charts is a geostrophic wind derived from highly smoothed fields of geopotential height. Satellite-derived winds computed in this manner and rawinsonde winds show similar circulation patterns except in areas of small height gradients. Magnitudes of the standard deviation of the differences between satellite-derived and rawinsonde wind speeds range from approximately 3 to 12 m s^{-1} on constant-pressure charts and peak at the jet-stream level.

Fields of satellite-derived surface wind computed with the logarithmic wind law agree well with fields of observed surface wind in most regions. Magnitudes of the standard deviation of the differences in surface wind speed range from approximately 2 to 4 m s^{-1}, and satellite-derived surface winds are able to depict flow across a cold front and around a low-pressure center.

17. KEY WORDS	18. DISTRIBUTION STATEMENT
Meteorological satellite data Satellite-derived soundings Satellite-derived winds	Unclassified - Unlimited Subject Category 47

19. SECURITY CLASSIF. (of this report)	20. SECURITY CLASSIF. (of this page)	21. NO. OF PAGES	22. PRICE
Unclassified	Unclassified	82	A05

For sale by National Technical Information Service, Springfield, Virginia 22161

NASA-Langley, 1981